Molecular Dynamics Simulations of Polymeric Nanocomposite Materials

by

Albert John Power

Heraklion 2015

ΠΑΝΕΠΙΣΤΗΜΙΟ ΚΡΗΤΗΣ
ΣΧΟΛΗ ΘΕΤΙΚΩΝ ΚΑΙ ΤΕΧΝΟΛΟΓΙΚΩΝ ΕΠΙΣΤΗΜΩΝ
ΤΜΗΜΑ ΕΠΙΣΤΗΜΗΣ ΚΑΙ ΤΕΧΝΟΛΟΓΙΑΣ ΥΛΙΚΩΝ

Ηράκλειο, 19 Ιουνίου 2015

Πρακτικά Εξεταστικής Επιτροπής
του Μεταπτυχιακού Φοιτητή *Πάουερ Αλβέρτου-Ιωάννη*
για την απόκτηση Μεταπτυχιακού Διπλώματος Ειδίκευσης

Ο ***κος Πάουερ Αλβέρτος-Ιωάννης,*** μεταπτυχιακός φοιτητής του Γενικού Μεταπτυχιακού Προγράμματος Μεταπτυχιακών Σπουδών του Τμήματος Επιστήμης και Τεχνολογίας Υλικών του Πανεπιστημίου Κρήτης, παρουσίασε υπό μορφή σεμιναρίου σε ανοικτό ακροατήριο στις **19 Ιουνίου 2015** την ερευνητική του εργασία με τίτλο :

«Προσομοιώσεις Μοριακής Δυναμικής Νανοσύνθετων Πολυμερικών Υλικών»

Η τριμελής εξεταστική επιτροπή έκρινε την εν γένει παρουσίαση και ερευνητική εργασία του υποψηφίου πολύ καλή και προτείνει ομόφωνα την απονομή του Μεταπτυχιακού Διπλώματος Ειδίκευσης.

Η Τριμελής Επιτροπή

Ρεμεδιάκης Ιωάννης (Επιβλέπων)
Μόνιμος Επίκουρος Καθηγητής Τμήματος Επιστήμης και Τεχνολογίας Υλικών
Πανεπιστημίου Κρήτης

Χαρμανδάρης Ευάγγελος
Επίκουρος Καθηγητής Τμήματος Μαθηματικών και Εφαρμοσμένων Μαθηματικών
Πανεπιστημίου Κρήτης

Αναστασιάδης Σπυρίδων
Καθηγητής, Τμήματος Χημείας
Πανεπιστημίου Κρήτης

Department of Materials Science & Technology,
School of Science, University of Crete, Greece

Master of Science Thesis

Molecular Dynamics Simulations of Polymeric Nanocomposite Materials

by

Albert John Power

Department of Materials Science and Technology, University of Crete, Heraklion , Greece
Institute of Applied and Computational Mathematics - Foundation for Research and Technology Hellas (FORTH), Heraklion, Greece

Master thesis committee:

Prof. Vagelis A. Harmandaris (Advisor)
Department of Mathematics and Applied Mathematics, University of Crete, Greece
Institute of Applied and Computational Mathematics - Foundation for Research and Technology Hellas (FORTH), Heraklion, Greece

Prof. Ioannis N. Remediakis
Department of Materials Science and Technology, University of Crete, Heraklion , Greece

Prof. Spiros H. Anastasiadis
Department of Chemistry, University of Crete, Heraklion, Greece
Institute of Electronic Structure and Laser - Foundation for Research and Technology Hellas (FORTH), Heraklion, Greece

Heraklion 2015

Table of Contents

ACKNOWLEDGMENTS

First and foremost, I would like to express my sincerest gratitude to my supervisor Prof. Vagelis Harmandaris for his endless support in all my studies and research, his patience and invaluable assistance and guidance.

Furthermore, I am also very thankful to the other members of the supervisory committee: Prof Ioannis N. Remediakis for the precious assistance and support he offered me at all levels and for providing us with the gold nanoparticle model and Prof. Spiros H. Anastasiadis for his encouragement, motivation and insightful comments.

I would also like to thank Dr. Anastassia Rissanou for our stimulating discussions and her significant guidance.

Moreover, I also thank all my colleagues from the Department of Materials Science & Technology and those from Prof. Vagelis Harmandaris's Group.

Special thanks to Ritsa Ieronymaki, MSc. for her invaluable assistance.

I would like to express my love and gratitude to my mother Melita by dedicating this thesis to her, and to thank her for her endless love and for her understanding throughout the duration of my studies.

My deepest gratitude to the Alexander S. Onassis Foundation for their Scholarship supporting my postgraduate studies and my warmest appreciation to everyone concerned as well as Mrs. Antigoni Maria Chantzolou of the Foundation's Department of Scholarships for Studies in Greece for her kind interest in my studies.

Last but not least, I would also like to thank the Institute of Applied and Computational Mathematics, IACM/FORTH, KRIPIS-PROENYL and THALES-AMOSICSS for their funding assistance.

ABSTRACT

The study of Polymeric Complex Materials is an intense research area due to the broad spectrum of systems, applications, length and time scales. For example, concerning hybrid Polymer/Solid systems, nanoparticles are used to modify/enhance the thermodynamics, the mechanical properties and the dynamical/rheological behavior of the entire system.

The aim of this work is to study the effect of gold, nanoparticles (NP) on polymer properties through detailed atomistic Molecular Dynamics, MD, simulations. In more detail, the structural, conformational and dynamical properties of polyethylene, PE, chains around an Au NP and a functionalized (Core/Shell) Au NP are investigated and compared to the behavior of bulk PE. Data concerning polymer density profiles, bond order parameter, segmental and terminal dynamics are reported. All polymer chain properties are examined as a function of distance from the Au NP. We find that the effect of the interface on density profile and conformational properties is from around 1.0 to 2.5 nm, whereas on local and global dynamics of polymer chains vary from around 2.0 to 4.0 nm.

1. INTRODUCTION

The study of model polymer nanocomposite systems [1-4], as well as general polymer–solid interfaces, at the molecular level is a very intense research area due to the development of hybrid materials, polymer coatings and lubricant films [5-8]. It is now accepted that the behavior of polymer melts close to a solid surface is rather different to the bulk behavior. For example, concerning the segmental dynamics of the macromolecules, a distribution of relaxation rates was found that depended largely on the strength of the polymer–surface interactions [9] whereas in some cases new dynamical modes appeared [10].

A lot of achievements both in basic research and in different industrial fields have been made on hybrid polymer/solid nanoparticle systems [11]. The most important concern the modification of the electrochemical behavior [12] and the improvement of the thermal degradation of the nanocomposites [13]. Moreover, enhancement of hardness, solvent resistance and glossiness of nanocomposites have been reported [14]. The improvement of the tensile strengths of nanocomposite films [15] and the enhancement of the interfacial adhesion between nanoparticle and polymer matrix are also of high importance [16]. Furthermore, nanoparticles modify the mechanical properties of a polymer matrix in the case of hybrid polymer/solid nanoparticle systems [17].

A range of simulations have been also employed to study the effect of the interface [3, 4], including dynamic Monte Carlo simulations for generic bead spring models [18, 19], united atom molecular dynamics (MD) simulations for alkanes [20-22], atomistic MD simulations [23, 24] and stochastic dynamics simulations of alkanes [25]. Bead–spring models using dynamic Monte Carlo simulations [26] and molecular dynamics [27] observed that segmental packing and orientation returned to bulk values within only a couple of segment lengths from the surface and chain dimensions returned to the bulk values after 1–2 times the radius of gyration R_g [28].

The goal of the present work is to predict the properties of hybrid polymer/gold systems at the molecular level through molecular simulations. Data concerning polymer density profiles, bond order parameter, segmental and terminal dynamics are

reported. Here, we study polyethylene (PE)/gold nanoparticle (Au NP) and functionalized (Core/Shell) PE/Au NP nanostructured systems. In more detail, the properties of polyethylene chains around a gold nanoparticle at a temperature of 450 K are investigated using atomistic molecular dynamics (MD) simulations. Several gold nanoparticles with Wulff construction were studied. The shape of Au nanoparticles has a key role in every aspect of their functionality, from sensing [29] and biolabeling applications [30] to plasmonics [31] and photonics [32]. Gold NPs diameter ranging from around 2.5–5 nm [33] and polyethylene chains consist of 22 monomers [22].

The present thesis is organized as follows:

- Chapter 2 gives a rather detailed presentation of the molecular dynamics method, with particular emphasis in its implementation for polymeric systems.
- Chapter 3 gives an overview of the molecular model for the polymer and the gold nanoparticle.
- Chapter 4 consists of a description for the simulated systems that we used and of the simulation method and analysis that we followed.
- Chapter 5 consists of the presentation of the results of the thesis. Data concerning polymer density profiles, bond order parameter, end to end distance, dihedral distribution, segmental and terminal dynamics, orientational and translational dynamics are reported. The polymer properties are examined as a function of distance from the Au NP and as an average value of the entire system.
- Chapter 6 presents the conclusions of the work of this thesis and recommendations for future plans.

2. MOLECULAR DYNAMICS

2.1 Molecular Dynamics Technique

Molecular dynamics (MD) is a powerful technique for computing the equilibrium and dynamical properties of classical many-body systems. Over the last twenty years, due to the rapid development of computers, polymeric systems have been the subject of intense study with MD simulations [18].

At the heart of this technique is the solution of the classical equations of motion which are integrated numerically to give information for the positions and velocities of atoms in the system [2, 3, 34]. The description of a physical system with the classical equations of motion rather than quantum-mechanically is a satisfactory approximation as long as the spacing hv between successive energy levels described is $hv < k_B T$. For a typical system at room temperature this holds for $< 0.6 \times 10^{13}$ Hz, i.e. for motions of time periods of about t > 1.6×10^{-13} sec or 0.16 ps.

A flow diagram of a standard MD algorithm is shown in Figure 1 and includes the following steps [35, 36].

- First, a model configuration representing a molecular-level snapshot of the corresponding physical system is chosen or constructed, and is initialized (initial positions, velocities of each particle within the system).
- Then the total force acting on each particle within the system is computed. For polymer systems such a force has two components: intermolecular (from atoms belonging to different polymer chains) and intramolecular (from atoms belonging to the same chain).
- The integration of the equations of motion follows with an appropriate method (like Verlet).
- Actual measurements are performed (positions, velocities, energies, etc., are stored) after the system has reached equilibration, periodically every N_k steps.
- After completion of the central loop (N steps), averages of the measured quantities and of the desired properties are calculated and printed.

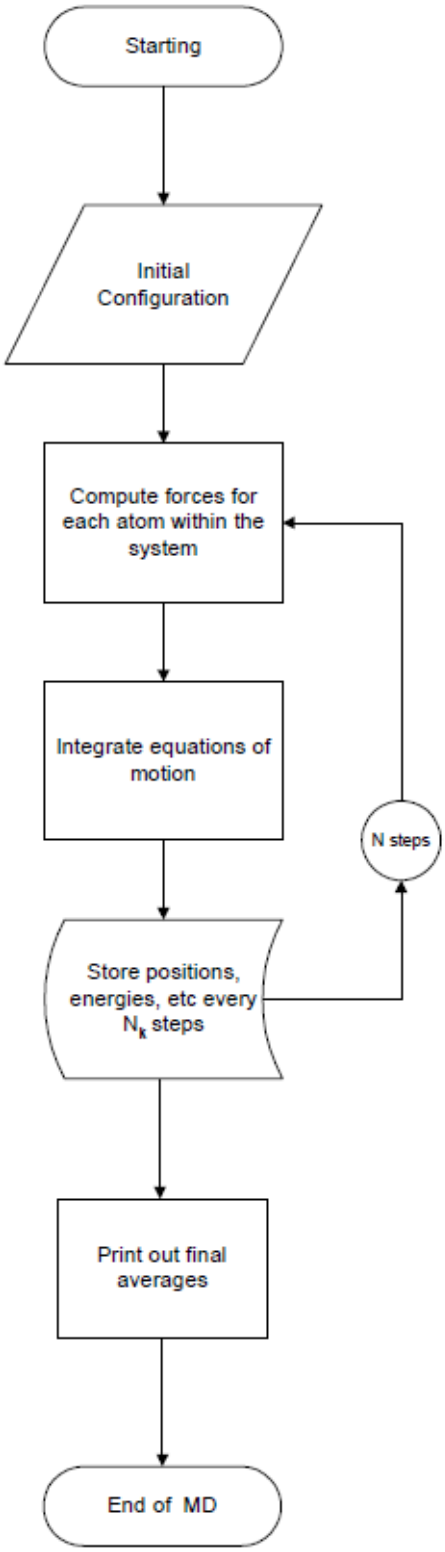

Figure 1: Diagram of a standard MD algorithm.

2.2 Classical Equations of Motion

As stated above, at the heart of an MD simulation is the solution of the classical equations of motion. Let us consider a system consisting of N interacting atoms described by a potential energy function $\boldsymbol{V}$. Let us also denote as q_k and $\dot{q}_k$ the generalized coordinates describing the molecular configuration and their time derivatives of particle k, respectively. The classical equations of motion for this system can be formulated in various ways [37]. In the Lagrangian formulation, the trajectory q(t)(= q_1(t), q_2(t), …, q_N(t)) satisfies the following set of differential equations:

$$\frac{\partial L}{\partial q_k} = \frac{d}{dt}\left(\frac{\partial L}{\partial \dot{q}_k}\right) \tag{1}$$

where L is the Lagrangian of the system. This is defined in terms of the kinetic, k and potential energy, V as

$$L = L(q, \dot{q}, t) \equiv K - V \tag{2}$$

The generalized momenta p_k conjugate to the generalized coordinates q_k are defined as

$$p_k = \frac{\partial L}{\partial \dot{q}_k} \tag{3}$$

Alternatively, one can adopt the Hamiltonian formalism, which is cast in terms of the generalized coordinates and momenta. These obey Hamilton's equations

$$\dot{q}_k = \frac{\partial H}{\partial p_k}, \dot{p}_k = -\frac{\partial H}{\partial q_k} \tag{4}$$

where H is the Hamiltonian of the system, defined through the equation

$$H(p,q) = \sum_k \dot{q}_k p_k - L \tag{5}$$

If the potential V is independent of velocities and time, then *H* becomes equal to the total energy of the system [37]:

$$H(p,q) = K(p) + V(q) \tag{6}$$

In Cartesian coordinates, Hamilton's equation of motion read:

$$\dot{r}_i \equiv v_i = \frac{p_i}{m_i} \tag{7}$$

$$\dot{p}_i = -\nabla_{r_i} V \equiv -\frac{\partial V}{\partial r_i} = F_i \tag{8}$$

hence

$$m_i \ddot{r}_i \equiv m_i \dot{q}_i = F_i \tag{9}$$

where F_i is the force acting on atom *i*. Solving the equations of motion then involves the integration of the 3N second-order differential equations (Newton's equations).

The classical equations of motion possess some interesting properties, the most important one being the conservation law. If we assume that K and V do not depend explicitly on time, and then it is straightforward to verify that $\dot{H} = dH/dt$ is zero, i.e. the Hamiltonian is a constant of the motion. In actual calculations this conservation law is satisfied if there exist no explicitly time or velocity-dependent forces acting on the system. A second important property is that Hamilton's equations of motion are reversible in time. This means that, if we change the signs of all the velocities, we will cause the molecules to retrace their trajectories backwards. The computer-generated trajectories should also possess this property.

There are many different methods for solving ordinary differential equations of the form of equation (9). Criteria for the proper choice of an algorithm include the following:

- Algorithm must not require an expensively large number of force evaluations per integration time step. Many common techniques for the solution of ordinary differential equations (such as the 4th order Runge-Kutta method) become inappropriate, since they do not fulfill this criterion.
- Algorithm should satisfy the energy conservation law. It is also desirable that it be time reversible and conserve volume in phase space (be symplectic).
- Algorithm should permit the use of a large time step dt.
- Algorithm should be fast and require little memory.

Concerning the solution of equations of motion for very long times, it is clear that no algorithm provides an essentially exact solution. But this turns out to be not a serious problem, because the main objective of an MD simulation is not to trace the exact configuration of a system after long time, but rather to predict thermodynamic properties as time averages and calculate time correlation functions descriptive of the dynamics [35, 36].

2.3 Verlet Methods

Algorithms in this family are simple, accurate and, as we will see below, time reversible. Thus, the Verlet methods are the most widely used methods for integrating the classical equations of motion. The initial form of the Verlet equations is obtained by utilizing a Taylor expansion at times t - dt and t + dt

$$r(t+dt) = r(t) + dtv(t) + \frac{dt^2}{2}\ddot{r}(t) + \frac{dt^3}{6} + O(dt^4) \tag{10}$$

$$r(t-dt) = r(t) - dtv(t) + \frac{dt^2}{2}\ddot{r}(t) - \frac{dt^3}{6} + O(dt^4) \tag{11}$$

Summing the two equations gives

$$r(t+dt) = 2r(t) - r(t-dt) + dt^2\ddot{r}(t) + O(dt^4) \tag{12}$$

with $\ddot{r}$(t) calculated from the forces at the current positions.

Two modifications of the Verlet scheme are of wide use. The first is the "leap-frog" algorithm where positions and velocities are not calculated at the same time; velocities are evaluated at half-integer time steps:

$$r(t+dt) = r(t) + dtv(t+\frac{dt}{2}) \tag{13}$$

$$v(t+\frac{dt}{2}) = v(t-\frac{dt}{2}) + dt\ddot{r}(t) \tag{14}$$

In order to calculate the Hamiltonian *H* at time t, the velocities at time t are also calculated as averages of the values at t + dt = 2 and t – dt = 2 :

$$v(t) = \frac{1}{2}(v(t+\frac{dt}{2}) + v(t-\frac{dt}{2})) \tag{15}$$

The problem of defining the positions and velocities at the same time can be overcome by casting the Verlet algorithm in a different way. This is the velocity Verlet algorithm according to which positions are obtained through the usual Taylor expansion

$$r(t+dt) = r(t) + dtv(t) + \frac{dt^2}{2}\ddot{r}(t) \tag{16}$$

whereas velocities are calculated through

$$v(t+dt) = v(t) + \frac{dt}{2}[\ddot{r}(t) + \ddot{r}(t+dt)] \tag{17}$$

with all accelerations computed from the forces at the configuration corresponding to the considered time. To see how the velocity-Verlet algorithm is connected to the original Verlet method we note that, by equation (17),

$$r(t+2dt) = r(t+dt) + dtv(t+dt) + \frac{dt^2}{2}\ddot{r}(t+dt) \tag{18}$$

If equation (17) is written as

$$r(t) = r(t+dt) - dtv(t) - \frac{dt^2}{2}\ddot{r}(t) \tag{19}$$

then, by addition, we get

$$r(t+2dt) + r(t) = 2r(t+dt) + dt[v(t+dt) - v(t)] + \frac{dt^2}{2}[\ddot{r}(t+dt) - \ddot{r}(t)] \tag{20}$$

Substitution of equation (18) into equation (20) gives

$$r(t+2dt) = r(t) = 2r(t+dt) + dt^2\ddot{r}(t+dt) \tag{21}$$

which is indeed the coordinate version of the Verlet algorithm (for more see [36]).

In general, higher-order methods are characterized by a much better accuracy than the Verlet algorithms, particularly at small times. Their biggest drawback is that they are not reversible in time, which results in other problems, such as insufficient energy conservation, especially in very long-time MD simulations. On the other hand, the Verlet methods are not essentially exact for small times but their inherent time reversibility guarantees that the energy conservation law is satisfied even for very long times. This feature renders the Verlet methods, and particularly the velocity-Verlet algorithm, the most appropriate one to use in long atomistic MD simulations.

2.4 MD in NVT and NPT ensembles

The methods described before consider the solution of Newton's equations of motion in a microcanonical (*NVE*) ensemble. In practice there is usually a need to perform MD simulations under specified conditions of temperature or/and pressure.

The thermostatting and barostatting is achieved by adding some dynamic variables which are coupled to the particle velocities (thermostatting) and simulation domain dimensions (barostatting). In addition to basic thermostatting and barostatting, we can also create a chain of thermostats coupled to the particle thermostat, and another chain of thermostats coupled to the barostat variables. The barostat can be coupled to the overall box volume, or to individual dimensions, including the *xy*, *xz* and *yz* tilt dimensions. The external pressure of the barostat can be specified as either a scalar pressure (isobaric ensemble) or as components of a symmetric stress tensor (constant stress ensemble). The time-averaged temperature and stress tensor of the particles will match the specified target values [38].

To constrain temperature, Nosé [39] introduced an additional degree of freedom, s, in the Lagrangian. The parameter s plays the role of a heat bath, whose aim is to damp out temperature deviations from the desirable level. This necessitates adding to the total energy an additional potential term of the form

$$V_s = gk_BTlns \tag{22}$$

and an additional kinetic energy term of the form

$$K_s = \frac{Q}{2}\left(\frac{\dot{s}}{s}\right)^2 = \frac{p_s^2}{2Q} \tag{23}$$

In the above equations, g is the total number of degrees of freedom (g = 3 N_{atoms} - N_{bonds} - 3 with N_{atoms} and N_{bonds} standing for the total numbers of atoms and bonds in the model system, respectively), while Q and p_s represent the "effective mass" and momentum, respectively, associated with the new degree of freedom *s*. Equations of motion are derived from the Lagrangian of the extended ensemble, including the degree of freedom *s*. Their final form, according to Hoover analysis [40] is

$$\dot{\boldsymbol{r}}_i = \frac{\boldsymbol{P}_i}{m_i} \tag{24}$$

$$\dot{\boldsymbol{P}}_i = -\frac{\partial V}{\partial \boldsymbol{r}_i} - \frac{\dot{s}}{s}\boldsymbol{P}_i \tag{25}$$

$$\dot{\boldsymbol{P}}_s = \frac{\left(\sum_{i=1}^{N}\frac{\boldsymbol{P}_i^2}{m_i} - gk_BT\right)}{Q} \quad , \quad \boldsymbol{P}_s = Q\frac{\dot{s}}{s} \tag{26}$$

An important result in Hoover's analysis is that the set of equations of motion is unique, in the sense that no other equations of the same form can lead to a canonical distribution.

The total Hamiltonian of the system, which should be conserved during the MD simulations, now becomes

$$H_{Nose-Hoover} = \sum_{i=1}^{N}\frac{\boldsymbol{P}_i^2}{m_i} + V(\boldsymbol{r}^n) + gk_BT\,lns + \frac{P_s^2}{2Q} \tag{27}$$

To construct MD simulations under constant P an analogous reformulation of the Lagrangian was proposed by Andersen [41]. The constant-pressure method of Andersen allows for isotropic changes in the volume of the simulation box. Later Hoover [40] combined this method with the isothermal MD method described before to provide a set of equations that probe MD simulations in the NPT ensemble. Parrinello and Rahman [42] have extended the Andersen method to allow the simulation box to respond not only to changes in its size but also in its shape. This is particular important in the simulation of solids (e.g. glassy polymers) since it allows for phase changes in the simulation involving changes in the dimensions and angles of the unit cell [35, 36].

3. THE IMPLEMENTATION OF THE MD METHOD

3.1 Molecular Model

For standard problems in physics and chemistry of condensed matter (such as simple fluids containing gas atoms or diatomic molecules) computer simulation considers a small region of matter in full atomistic detail [3]. For simple fluids these methods works because they are homogenous on a scale of about 1-2 nm already. Reliable model for the effective forces are usually available from quantum chemistry methods.

MD simulations in long flexible polymers encounter a different situation due to the wide spread of length scales characterizing their structure and time scale characterizing their motion as we show in the introduction. As we have already seen in the introduction one solution to the problem of long relaxation times is to follow hierarchical approaches that are using combination of simulation techniques and theories. A different solution to the above problems is to abandon the chemical detail and concentrate in the dynamics of long wavelengths. This is the case of coarse-graining simulations.

Consider a polyethylene chain in full atomistic representation as the one shown in Figure 2.

There are two ways of treating the hydrogen atoms. The one is to treat them explicitly, i.e. explicit atom (EA) models. The second is to introduce spherical segments, as in Figure 2a, representing a CH_2, i.e. united atom (UA) models. There are two types of interactions in this atomistic representation. The first is between atoms that are bonded or next near up to n bonds (bonded interactions). The second one is between atoms that are belonging to different polymeric chains or to the same chain but their distance is above n bonds (non-bonded interactions) [18].

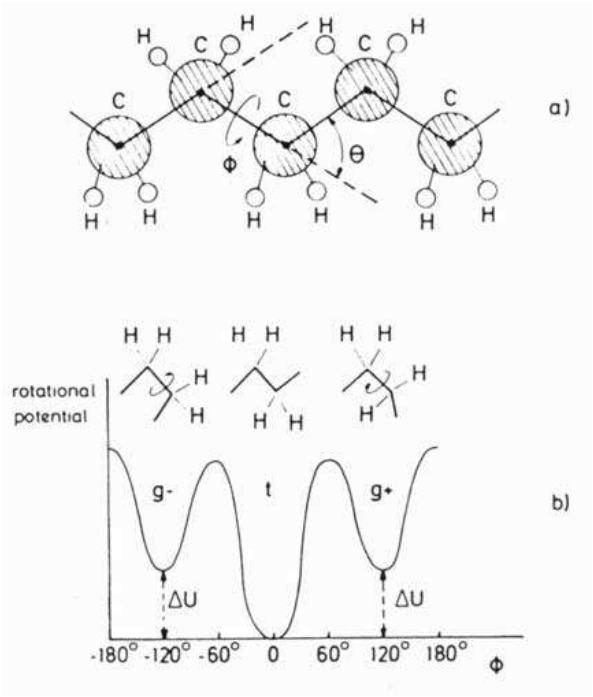

Figure 2: (a) Schematic model of a piece of the polyethylene chain in the united atom representation. (b) Qualitative sketch of the torsional potential for alkane chains.

The equation that describes the molecular interactions (see Figure 3) between atoms is:

$$U(r) = V_{bonded} + V_{non-bonded} = V_{str} + V_{bend} + V_{tors} + V_{LJ} + V_q \qquad (28)$$

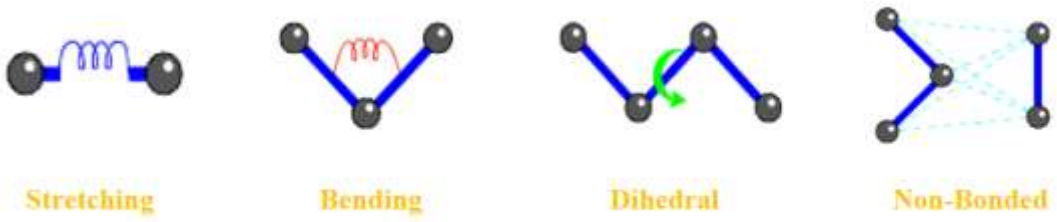

Figure 3: Molecular interactions between atoms

The bonded interactions depend on the type of the polymeric systems. There are, however, three general types of bonded interactions:

a) Interactions between atoms that are connected through a bond. The interaction of the chemical bond can be incorporated through a harmonic potential (bond stretching interaction) of the form

$$V_{str}(l) = \frac{1}{2} k_b (l - l_0)^2 \tag{29}$$

where l is the bond length and l_0 is its equilibrium value.

b) For atoms that are belonging to 2 successive bonds a bond-bending potential of the following form is used

$$V_{bend}(\theta) = \frac{1}{2} k_\theta (\theta - \theta_0)^2 \tag{30}$$

where θ is the bond length and θ_0 is its equilibrium value.

c) For atoms that are belonging to 3 successive bonds (see Figure 2b) there is a torsional potential, associated with each dihedral angle φ. The type of the torsional potential is usually of the form

$$V_{tors}(\phi) = \sum_{i=0}^{n} c_i (\cos(\phi))^i \tag{31}$$

with n around 3-5 and c_i constants characterizing the potential.

For systems with special types of interactions (double bonds, hydrogen bonds, special dihedral angles, etc.) there are other much more detailed and complicated types of bonded interactions [18].

The non-bonded interactions are usually of two types:

a) The first are short-range interactions. These interactions are between atoms belonging to different chains or atoms that are in the same chain but they are separated by more than n (usually 3) bonds apart and have the following Lennard-Jones (LJ) form

$$V_{LJ}(\boldsymbol{r}) = 4\varepsilon \left[\left(\frac{\sigma}{\boldsymbol{r}} \right)^{12} - \left(\frac{\sigma}{\boldsymbol{r}} \right)^{6} \right] \tag{32}$$

where ε and σ are parameters characteristic of the type of the atom. The parameters between different types of sites (atoms) are usually determined by the Lorentz-Berthelot rules:

$$\varepsilon_{CH_2-CH_3} = \sqrt{\varepsilon_{CH_2}\varepsilon_{CH_3}}\ , \qquad \sigma_{CH_2-CH_3} = \frac{\sigma_{CH_2} + \sigma_{CH_3}}{2} \tag{33}$$

b) The second type of non-bonded interactions is the well-known long-range Coulomb interactions [43]. Consider a number of atoms N in a cubic box of length L. If periodic boundary conditions are applied and we assume that the system as a whole is electrically neutral, then the Coulomb contribution to the potential energy of this system is

$$V_q = \frac{1}{2}\sum_{n\in\mathbb{Z}^3}^{\infty}\sum_{i,j=1}^{N}{}', \frac{q_i q_j}{|r_{ij}+nL|} \tag{34}$$

where $r_{ij} = r_i - r_j$, q_i and q_j are the charges, the first sum is over all periodic images n and the prime denotes that the summand for i = j has to be omitted for n = 0. For simulating systems with long-range interactions special simulation techniques needed, such as the Ewald summation, the particle-particle-particle mesh (PPPM) method or the fast multipole method [2, 43].

3.2 Gold Nanoparticle - Wulff Construction

Gold nanoparticles are often found in their equilibrium shape [33, 44, 45]. At the thermodynamic limit, this is a polyhedron enclosed by faces of various (*hkl*) crystal orientations such that the total surface energy is minimum

$$\sum_{hkl} A_{hkl}\gamma_{hkl} \tag{35}$$

A_{hkl} is the total area of faces parallel to the (*hkl*) plane of the crystal and γ_{hkl} is the energy required to create a surface of unit area that is parallel to the (*hkl*) plane of the crystal and is the analog of the surface tension of liquids.

The Wulff construction has been used to predict equilibrium shapes in a variety of systems [46-48]. G. Wulff proposed that the shape that minimizes equation (35) is such that the distance of each face from the center is proportional to the surface tension of the respective (*hkl*) surface [48]:

$$d_{hkl} \sim \gamma_{hkl} \tag{36}$$

Prof. Ioannis N. Remediakis and G.D. Barmparis [33] predicted the equilibrium shapes of gold nanoparticles by linking extensive quantum-mechanical calculations, based on density functional theory (DFT), to Wulff constructions. They constructed atomistic models of nanoparticles with diameters up to several tenths of a nanometer, inaccessible by direct atomistic simulations. The Wulff construction [33] for Au NP is shown in Figure 4.

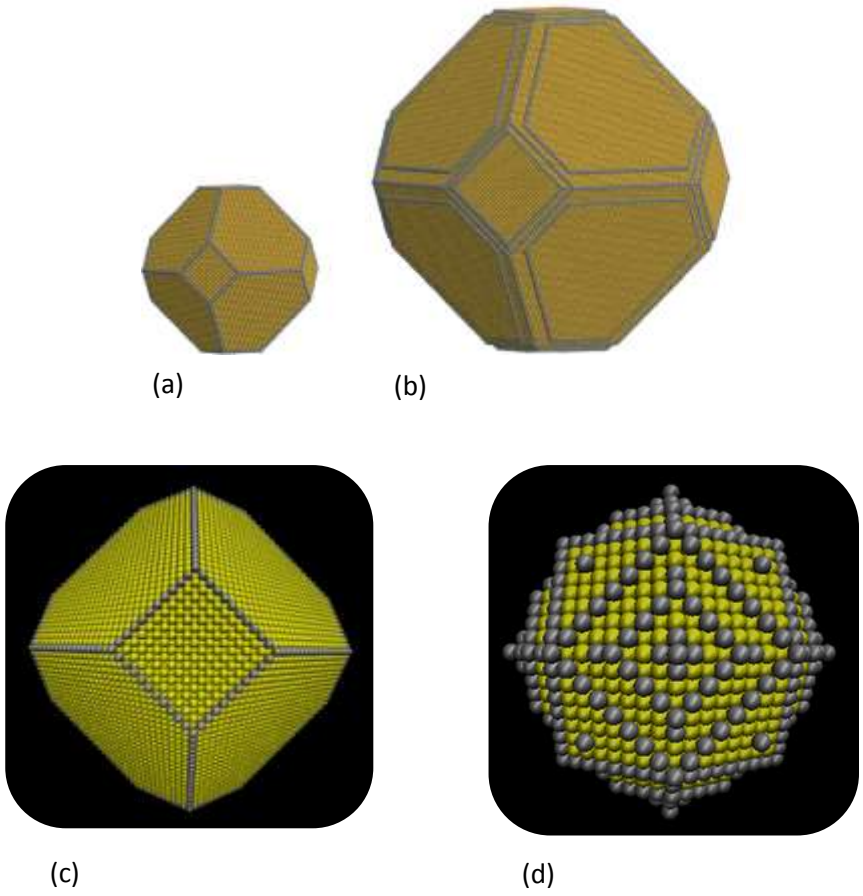

Figure 4: Typical calculated Au nanoparticles for various sizes, *d*: (a) *d* = 12.1 nm (b) *d* = 27.2 nm, (c) *d* = 5.02 nm and (d) *d* = 5.04 nm (for the grafted system). Step and kink atoms are shown in darker color.

4. SIMULATION OF HYBRID PE/GOLD NP SYSTEMS

4.1 Simulated Systems

The polyethylene matrix [22] that we used has 5040 chains with 22 monomers per chain and in total 110880 CH_2/CH_3 United-Atoms [49].

- In the 1st case two different gold NPs with Wulff construction were modeled [33]; one with diameter of 25 Å and one with 50 Å.

- In the 2nd case we used the same polymer matrix but different nanoparticle. Both of the grafted Au nanoparticles have diameter of 5 nm and 53 grafted polyethylene chains. The first one has 20 monomers per chain and the other one 62 monomers per chain. The grafting density is 0.67 chains per square nm.

More details for all systems are presented in Table 1. Typical snapshots of the PE/Au NP and the Core/Shell PE/Au NP systems are shown in Figure 5 and Figure 6 respectively.

Name	Au NP Diameter	Au Atoms	Free PE Monomers	Free PE Chains	Au/PE wt%	Grafted PE Chains	Grafted PE mers/chain
S1	25.1 Å	459	110880	5040	5.8	-	-
S2	50.2 Å	3101	110880	5040	38.8	-	-
S3	50.4 Å	2461	110880	5040	30.8	53	20
S4	50.4 Å	2461	110880	5040	30.8	53	62
SB	-	-	9240	420	-	-	-

Table 1: Details for the simulated systems.

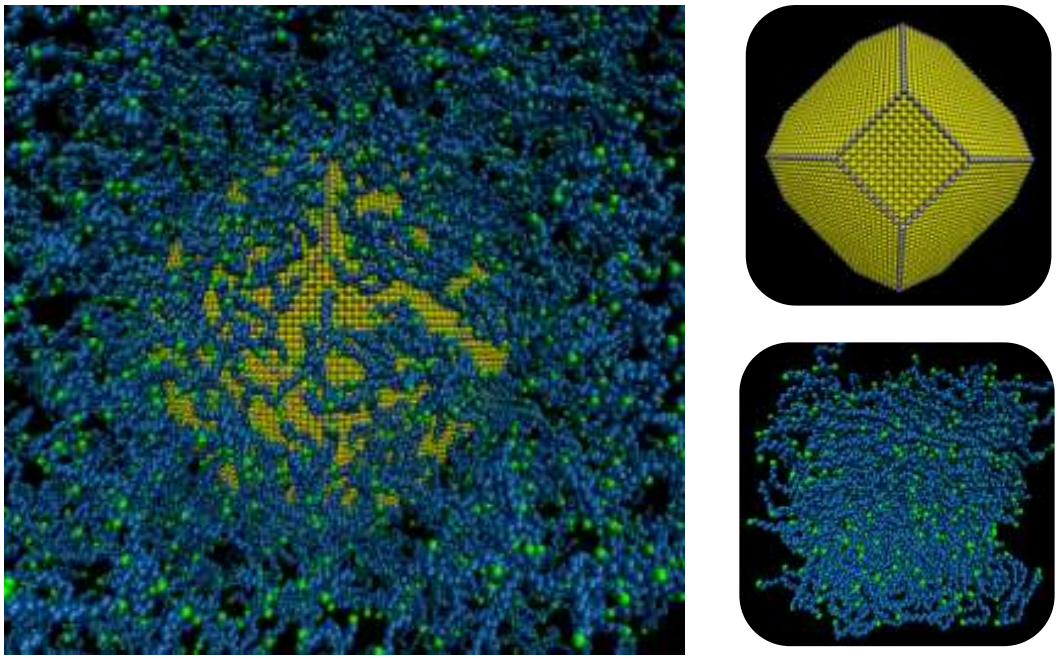

Figure 5: Snapshot from MD simulation of hybrid polyethylene/gold nanoparticle at 450K. Au nanoparticle (3101 atoms, diameter of 5.02 nm) and polyethylene (5040 chains, 22-mers per chain) are shown. With yellow is the Au and with grey are the edges of Au nanoparticle. With blue are the CH_2 and with green the CH_3 monomers.

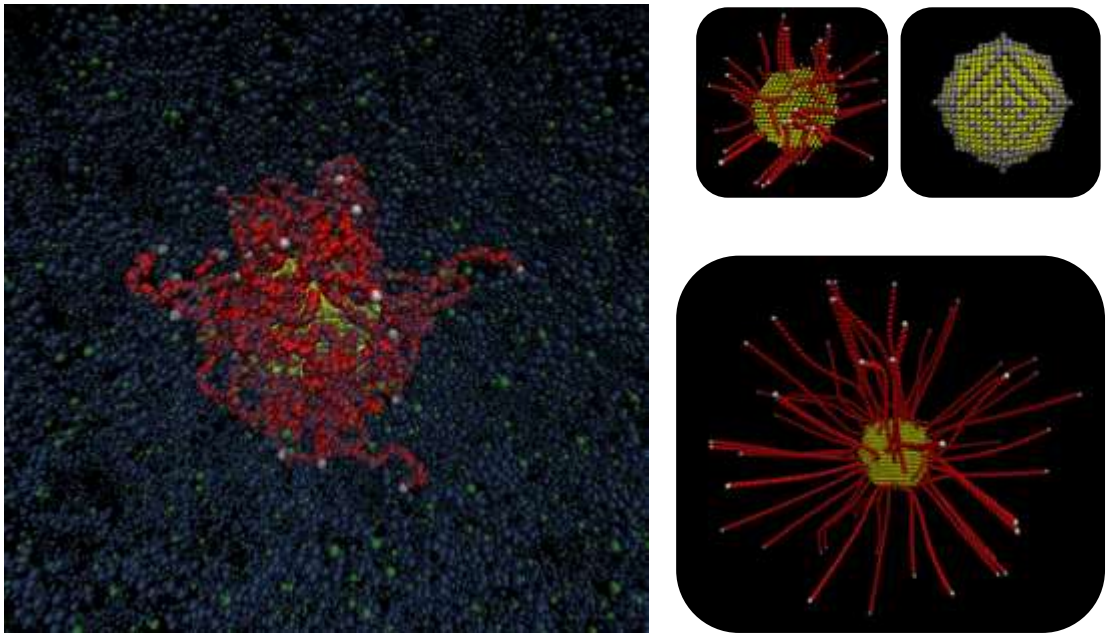

Figure 6: (Left) Snapshot from MD simulation of hybrid polyethylene/grafted gold nanoparticle at 450K. Au nanoparticle (2461 atoms, diameter of 5.04 nm) and polyethylene (5040 chains, 22-mers per chain) are shown. With yellow is the Au and with grey are the edges of Au nanoparticle. With blue are the free CH_2 and with green the free CH_3 monomers. With red are the grafted CH_2 and with white the grafted CH_3 monomers. **(Right)** The grafted Au NP without the brushes and the initial configuration of the grafted NP with the short brushes and with the long brushes.

4.2 Simulation Method

The methodology that we follow is applicable to various polymer/solid interfacial systems and model polymer nanocomposite. It consists of the following stages:

- The 1st step is the generation of initial structure.
- The 2nd step is the equilibration of the hybrid system through energy minimization and long simulation runs.
- The 3rd step is the execution of Molecular Dynamics simulations for times up to 30 ns.
- The final step is the estimation of properties for the entire hybrid systems and detailed analysis of polyethylene/NP interfaces.

Molecular Dynamics (MD) simulations were performed in the isothermal-isobaric (NPT) statistical ensemble, using the LAMMPS package [38]. The pressure was kept constant using Nosé Hoover barostat at P = 1 atm. The Nosé Hoover thermostat was used to maintain the temperature at T = 450 K. The integration time step was 1.0 fs and periodic boundary conditions have been used in all three dimensions.

The system has 5040 molecules of polyethylene with 22 monomers per chain. For the representation of polyethylene a united atom model was used, where each methylene CH_2 and methyl CH_3 group was considered as a single Van der Waals interacting site. The polyethylene bonds and angles described by harmonic potential and the dihedrals by the OPLS force field (Table 2). For the Van der Waals interactions between the PE-PE (Table 3) we used a spherically truncated 6–12 Lennard–Jones potential with cutoff distance R_c = 10 Å [22].

The first gold nanoparticle with Wulff construction has 459 atoms with 2.51 nm diameter and the second has 3101 atoms with 5.02 nm diameter [33]. The gold nanoparticles are frozen and for the Van der Waals interactions between the Au-PE we used the Morse potential with cutoff distance R_c = 10 Å (Table 2).

For the Core/Shell Au NP systems [50], the minimum distance between the Au and the Sulfur is 1.7 Å. A harmonic potential is used to describe the thermal fluctuations associated with the Au-S-CH_2 angle. For the interactions between the S-PE (Table 3)

Non-Bonded Interactions

$$V_{LJ}(r_{ij}) = 4\varepsilon_{ij}\left[\left(\frac{\sigma_{ij}}{r_{ij}}\right)^{12} - \left(\frac{\sigma_{ij}}{r_{ij}}\right)^{6}\right], r \leq R_c$$ **Lennard-Jones**

Atom Types	mass (g/mol)	σ (nm)	ε (kJoule/mol)
CH_2	14.027	0.395	0.3824
CH_3	15.035	0.395	0.3824
S - CH_2	32.066 - 14.027	0.372	0.7219
S - CH_3	32.066 - 15.035	0.372	0.8761

$$V_{Morse}(r_{ij}) = D_0\left[e^{-2a(r-r_0)} - 2e^{-a(r-r_0)}\right], r \leq R_c$$ **Morse**

Atom Types	mass (g/mol)	D_0 (kJoule/mol)	α (nm^{-1})	r_0 (nm)
Au - CH_2	196.967 - 14.027	1.6885	11.69	0.4085
Au - CH_3	196.967 - 15.035	1.6885	11.69	0.4085

Table 2: Model parameters and functional forms of all non-bonded interactions of the atomistic force field.

Bonded Interactions

$$V_b(r_{ij}) = \frac{1}{2}k_{ij}^b\left(r_{ij} - b_{ij}\right)^2$$

Bond	b (nm)	k^b (kJ/mol·nm^2)
$CH_2 - CH_2$	0.154	100,000.00
$CH_2 - CH_3$	0.154	100,000.00
$CH_3 - CH_2$	0.154	100,000.00

$$V_\alpha(\theta_{ijk}) = \frac{1}{2}k_{ijk}^\theta\left(\theta_{ijk} - \theta_{ijk}^0\right)^2$$

Angle	θ° (deg)	k^0 (kJ/mol*rad^2)
$CH_2 - CH_2 - CH_2$	114	519.611
$CH_3 - CH_2 - CH_2$	114	519.611
$CH_2 - CH_2 - CH_3$	114	519.611
S - $CH_2 - CH_2$	114	519.611

$$V_{opls}\left(\varphi_{ijkl}\right) = \frac{1}{2}K_1[1+\cos(\varphi)] + \frac{1}{2}K_2[1-\cos(2\varphi)] + \frac{1}{2}K_3[1+\cos(3\varphi)] + \frac{1}{2}K_4[1-\cos(4\varphi)]$$

Dihedral	K_1 (KJ/mol)	K_2 (KJ/mol)	K_3 (KJ/mol)	K_4 (KJ/mol)
CH_3–CH_2–CH_2–CH_2	4.276	-1.12968	13.1545	0.00
CH_2–CH_2–CH_2–CH_2	4.276	-1.12968	13.1545	0.00
CH_2–CH_2–CH_2–CH_3	4.276	-1.12968	13.1545	0.00
S- CH_2–CH_2–CH_2	4.276	-1.12968	13.1545	0.00

Table 3: Model parameters and functional forms of all bonded interactions of the atomistic force field.

we used a 6–12 Lennard–Jones potential with cutoff distance R_c = 10 Å. For the S-CH_2-CH_2CH_2 dihedral angle interactions the OPLS force field was used (Table 2).
Tail corrections were applied to both energy and pressure. For the non-bonded interactions between PE-PE monomers, the Lorentz–Berthelot rules were used.

In order to obtain initial PE/Au configurations, first we randomly added the brushes to the Au surface. Next, energy minimization to the Core/Shell system was executed and then MD simulation run up to 10 ns in NVT ensemble was performed. Finally, the Au nanoparticle, grafted or not, was placed at a close distance (about 0.5 nm) to several well-equilibrated polymer samples [22].

For the equilibration of the systems, first MD (Molecular Dynamics) simulations for 30 ns were performed, during which the motion of the overall hybrid system was monitored. This time period is much larger than the time required for the de-correlation of PE end-to-end vector (about ~100 ps) [22].

Then production runs for times up to 30 ns were performed and several PE/Au NP configurations were saved. In data analysis we exclude a certain number of configurations such as our results to be independent of the initial state.

In a further step, all configurations that were gathered during the simulation runs were analyzed in a post processing procedure. Of particular importance are the heterogeneous characteristics of the hybrid systems, due to distribution of polymer/gold NP intermolecular (adhesive) interactions. Therefore, properties of the polymer chains were examined as a function of the distance from the Au NP, as it was shown in our previous work [21].

4.3 Analysis

The structural, conformational, and dynamical properties of the chains were analyzed and compared to the behavior of the bulk polyethylene system. In more detail, we report data concerning polymer density profiles, bond order parameter, segmental and terminal dynamics. Our main goal is to study the spatial and dynamical heterogeneities of model hybrid polymer/nanoparticle systems in a detailed way at the molecular level. The reported data could be very useful for the prediction of the properties, as well as for the design, of such materials, in particular since typical

experiments are not able to distinguish easily between the interface at the solid surface and the free surface and, therefore, the measured properties are an average value of the entire system.

The analysis presented here has been performed along radial distances from the center of mass of the gold NP, by creating spherical shells of increasing radius (*i.e.*, increasing distances form the Au NP). This calculation has to be repeated at every time step. A sketch of this analysis scheme is depicted in Figure 7.

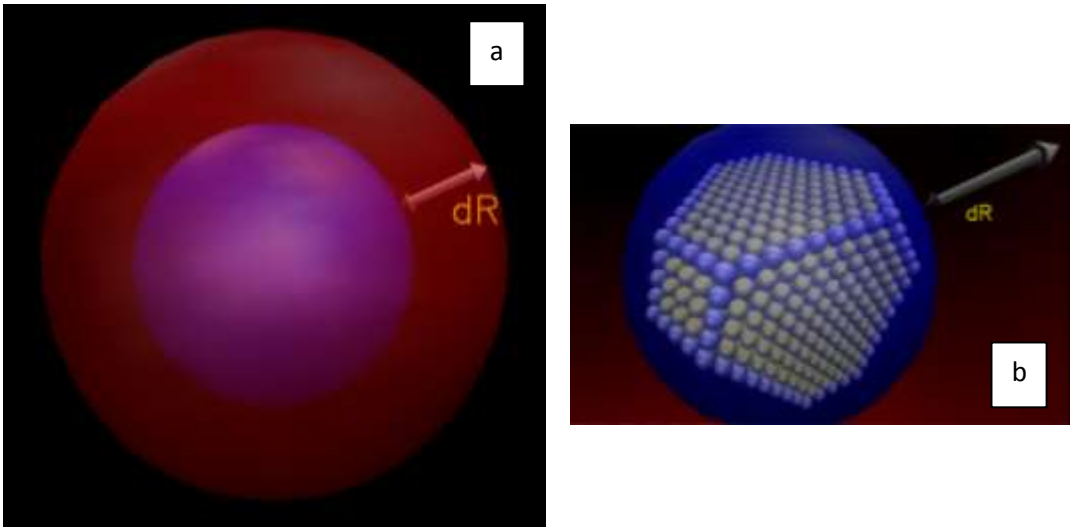

Figure 7: a) A sketch of the analysis scheme in spherical shells. **b)** Inside view of the Figure(a).

The mass density profiles were calculated according to the above-discussed radial distance, using spherical shells of thickness equal to 1 Å. The same binning was used for the calculation of the second rank bond order parameter. Thicker spherical shells were used for the calculation of dynamical properties, of around 5 - 10 Å for both orientational and translational dynamics in the segmental level in order to improve statistics, whereas a 15 - 20 Å binning was used for the distribution of atoms according to their mean squared displacements in each shell. The choice of binning size (thickness of spherical shells) for the computation of each specific property is the result of an optimized balance between detailed information and improved statistics.
Furthermore, for the calculation of the density of PE as a function of the distance from the nanoparticle we applied the following procedure: The volume of each spherical shell is equal to:

$$V_{shell} = \frac{4}{3}\pi\left[\left(r+dr\right)^3 - r^3\right] \tag{37}$$

where r is the radius of a sphere, centered at the center of the gold NP and dr is the thickness of the shell. Then the polymer number density is given by:

$$\rho_{PE} = \frac{N_{PE}}{V_{shell}} \tag{38}$$

where N_{PE} is the number of PE atoms in the shell.

5. RESULTS

Four different Au NPs have been modeled (systems S1, S2, S3 and S4 see Table 1) as well as a bulk PE system (SB) in the same conditions (temperature and pressure) in order to compare the properties of the Hybrid system with the unperturbed bulk one. Representative snapshots of the modeled systems are shown in Figure 5 and Figure 6.

5.1 Density Profile

We start the analysis of the hybrid model with the calculation of the mass monomer density profile of the polymer (PE) chains as a function of the distance from the gold NP. Average density profiles, which have been calculated for the center of mass of the monomers, $\rho(r)$, are presented in Figure 8 for all systems.

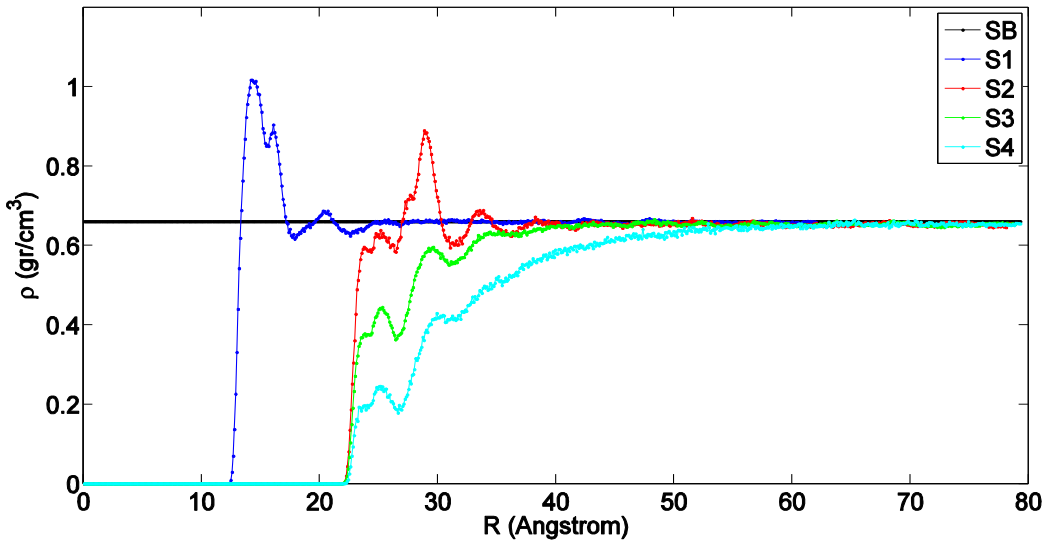

Figure 8: Mass monomer density profiles of polyethylene as a function of *r* (distance from the center of the gold NP) for the five systems.

In Figure 8, the polymer mass at each spherical shell has been divided with the total volume of the shell, which for the inner shells contains only Au atoms, whereas the outer shells contain only polymer atoms. Away from the Au NP, all curves reach/approach the bulk density value, though at different distances, as a result of the nanoparticle dimensions.

S1 and S2 systems exhibit the same behavior: a peak of rather similar height (larger than the bulk value) is observed at a distance/radius of about 1.3 nm and 1.8 nm

respectively, which denotes the attraction of the polymer from the gold NP at short distances, while at longer distances the bulk density is attained. In the Core/Shell Au NP system (S3 and S4), only few polyethylene chains can penetrate the brushes and reach the gold surface.

For the Core/Shell NP system, the density profile can be decomposed to free polyethylene chains and grafted polyethylene chains. In Figure 9, with green and light blue is the free polyethylene, with magenta and blue is the grafted polyethylene and with red and yellow is the summation of free and grafted polyethylene. We observe that the density values for the free polyethylene chains are lower than the corresponding bulk value close to the surface due to the nanoparticle's brushes, which do not allow the interpenetration. However, the NP with short brushes allows more free PE chains to reach close to the surface compared to the case of long brushes NP. On the other hand for the grafted polyethylene chains (i.e., S3 and S4 systems) we observe a peak close to the Au NP due to the attraction from the surface. This peak is more pronounced for the case of S4 system due to the longer brushes. Moreover, the extension of brushes is up to 35 Å and up to 55 Å for the S3 and S4 systems respectively. Therefore, the corresponding bulk values are attained at these distances, as is observed in the density profiles of the total density curves (sum of free and grafted polyethylene chains).

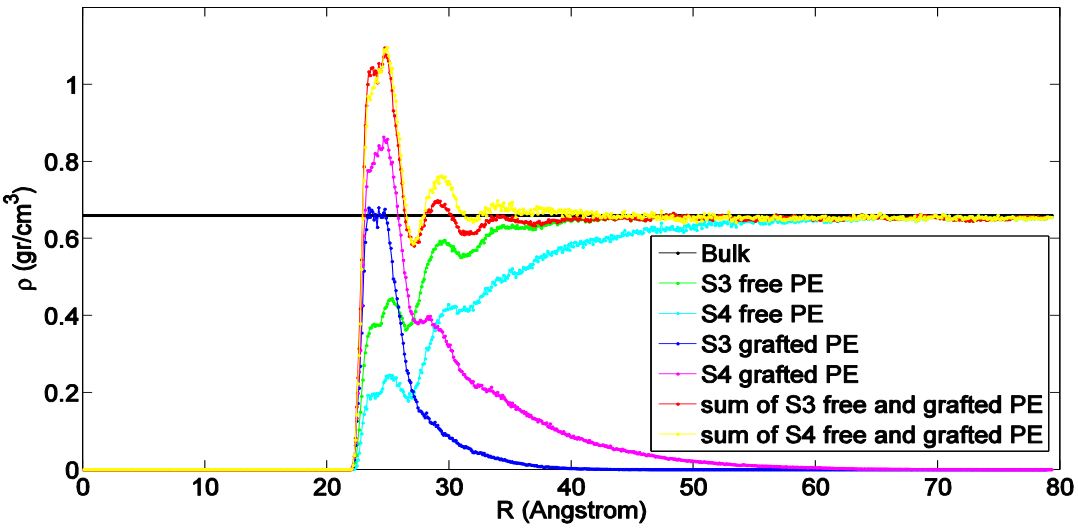

Figure 9: Mass monomer density profiles of polyethylene as a function of *r* (distance from the center of the gold NP) for the S3 and S4 systems. The density profile was decomposed to free polyethylene chains and grafted polyethylene chains.

5.2 Orientational Properties at the Monomer Level

In the following we examine the orientation of the polymer chains close to the gold NP in the segmental level through the $\boldsymbol{v}^{1-3}$ vector which connects two non-consecutive carbon atoms (see Figure 10Figure 10). In more detail, the second rank bond order parameter [1, 51] is calculated. Defined as:

$$P_2(\cos\theta) = \frac{3}{2}\langle \cos^2\theta \rangle - \frac{1}{2} \tag{39}$$

$P_2(\cos\theta)$ limiting values of −0.5, 0.0, and 1.0 correspond to perfectly parallel, random, and perpendicular vector orientations relative to the Au NP, respectively. In the above formula θ is the angle between the vector, which is defined along the molecule (here the $\boldsymbol{v}^{1-3}$ one) and the radial distance from the center of gold NP.

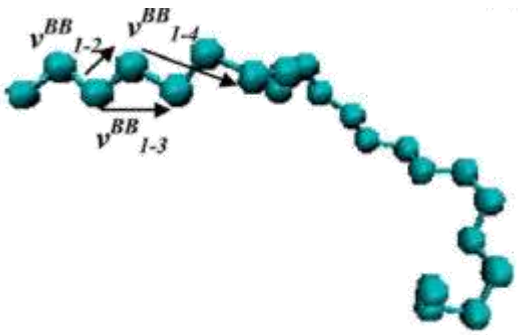

Figure 10: Snapshot of oligomers of PE chain. Characteristic vectors along the backbone and from the backbone to the side groups are drawn.

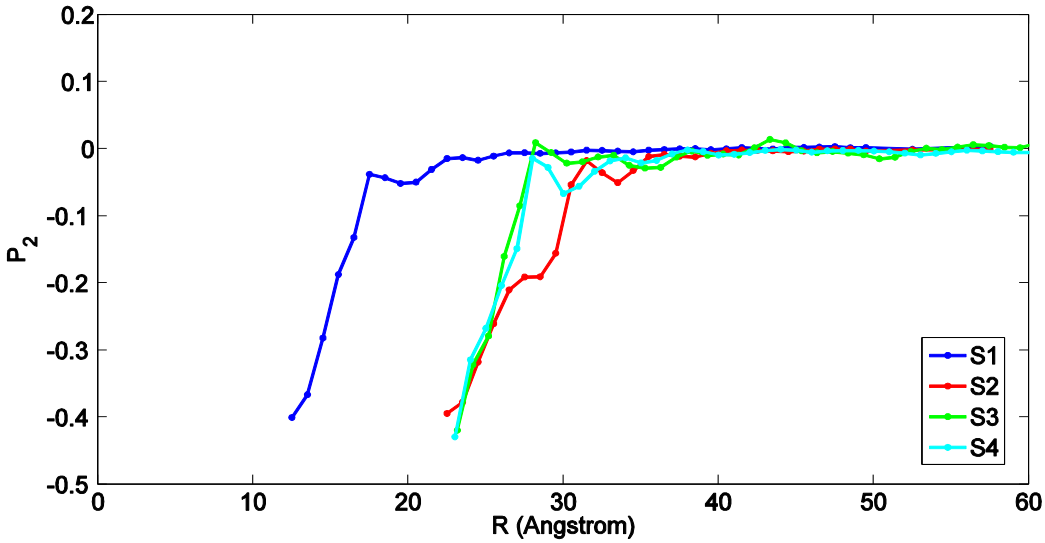

Figure 11: Second rank bond order parameter P2(cos(θ)) of polyethylene for v^{1-3} vector as a function of R distance (distance from the center of the Au NP) for all polymer/gold nanoparticle systems.

The bond order parameter of $\boldsymbol{v}^{1-3}$ for all systems is depicted in Figure 11. In all cases there is an obvious tendency of the segments of the polymer chain for an almost parallel to the gold NP orientation at short distances which is gradually randomized with the distance. There is a decrease of the bond order parameter of the PE segments closest to the Au NP and the minimum values are about −0.4 for all hybrid systems.

5.3 Conformational Properties

We start the analysis of the chain conformations by calculating the average chain end-to-end distance

$$R_{ee} = \left\langle R_{ee}^2 \right\rangle^{1/2} \tag{40}$$

An important question concerns whether chain swelling occurs due to chain adsorption at the polymer/nanoparticle interface. Our approach for the sorting of the R_{ee} vector in the different adsorption spherical shells with respect to the surface is based on the center of mass of the corresponding vector. Note here that this approach for the case of the end-to-end vector might lead to selection bias, since only chains with a rather flat conformation will have their center of mass near the gold NP surface. An alternative approach would be to compute the mean R_{ee} for each distance from the gold nanoparticle by averaging over the R_{ee} for all chains, with a weighting assigned to each chain based on the fraction of monomers at a given distance from the Au NP that they belong to.

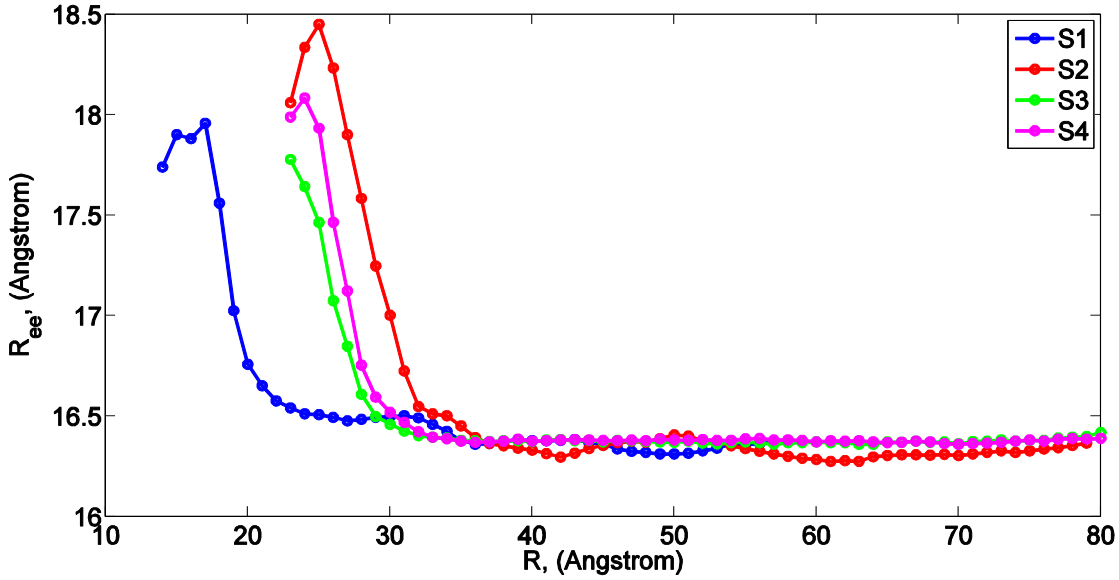

Figure 12: Average chain end-to-end distance, R_{ee} for chains belonging in different adsorption layers, *R*.

The end-to-end distance of the polymer chains as a function of distance from the Au NP is shown in Figure 12. As we can see chain dimensions are rather similar at all distances (and same to the bulk values) except the first layers where an increase of the R_{ee} are observed. However this increase is rather small, only about 10% of the bulk values. Error bars are 3%–5% of the actual values based on block averaging techniques. In Figure 12 we observe that close to the gold NP, S1 system attains lower R_{ee} values in comparison to S2 due to the S1's smaller surface area. In addition S2 attains bigger R_{ee} values in comparison to S3 and S4 systems due to the core/shell NP's brushes.

A further analysis of the PE chain conformations is based on the calculation of the distribution of the torsional (dihedral) angles, P_{dih}, in different distances from gold NP. This is of particular importance since for PE the distribution of its (backbone) dihedral angle is critical for the determination of its overall chain conformation. In the analysis performed here all torsional angles with value 0°, are defined as "trans", −60° and +60° as "gauche-" and "gauche+" respectively and 180° as "cis". Our results which are depicted in Figure 13 and Figure 14 indicate clear spatial heterogeneous dihedral angle distribution, for S1 and S2 hybrid systems. For the first adsorption layers a non-negligible enhancement of the trans states with a consequent reduction of the gauche ones is observed for all systems compared to the bulk case. This observation reflects the more ordered PE chains close to the gold NP. Enhancement of

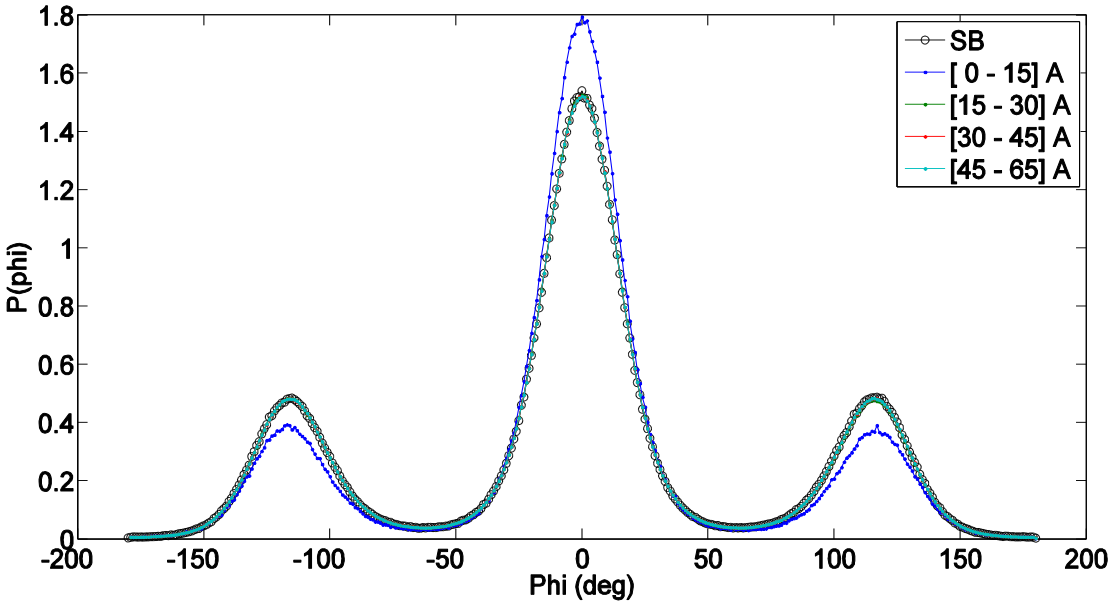

Figure 13: Torsional angles distribution as a function of R distance (distance from the center of the gold NP). All spherical shells of the (S1) system and the corresponding bulk curve.

"trans" population would be expected to affect the crystallinity of PE chains as well as the mechanical properties of the hybrid system. Moreover no differentiation in the torsional angle distributions among the S3 and S4 systems is detected (Figure 15 and Figure 16). For the most distant adsorption layer (*i.e.*, bulk region), the curves are completely identical to each other and to the corresponding bulk one. Overall, the distance above which all P_{dih}'s become similar to the bulk P_{dih} defines the width of the interphase for the particular property.

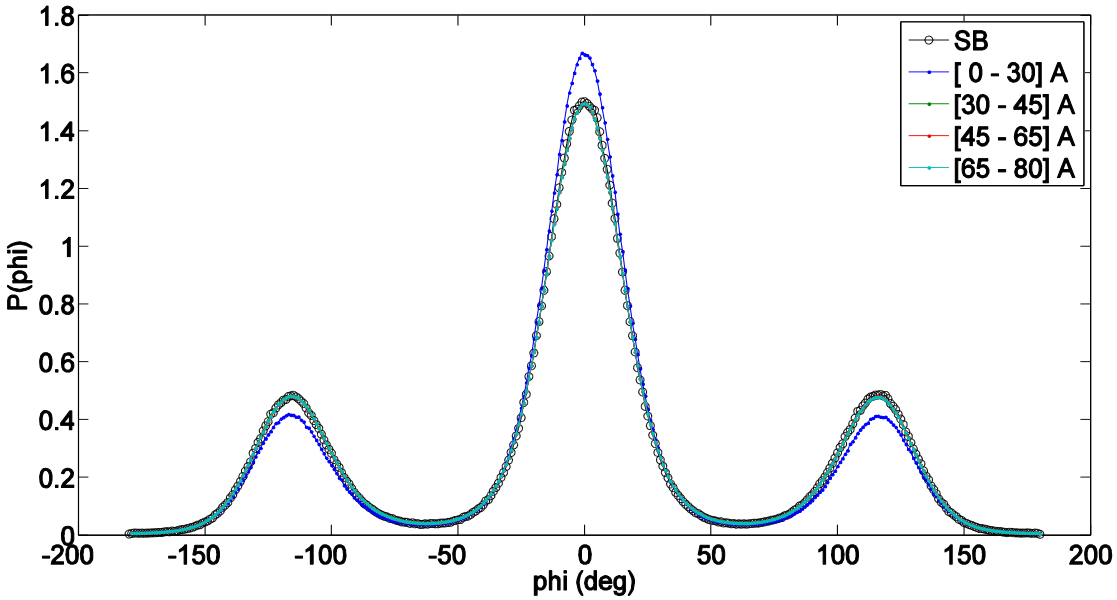

Figure 14: Torsional angles distribution as a function of R distance (distance from the center of the gold NP). All spherical shells of the (S2) system and the corresponding bulk curve.

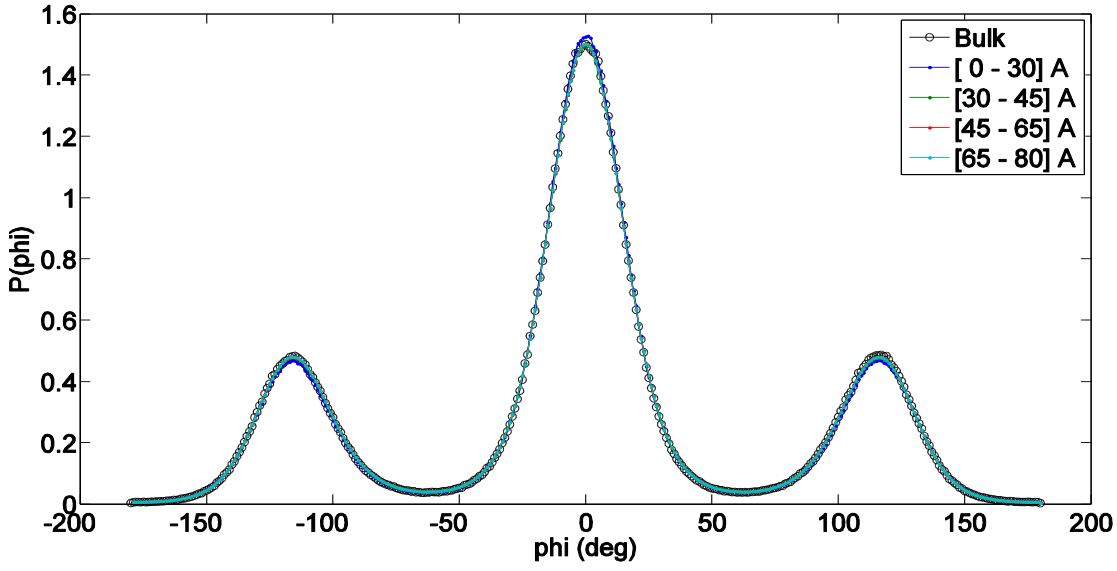

Figure 15: Torsional angles distribution as a function of R distance (distance from the center of the gold NP). All spherical shells of the (S3) system and the corresponding bulk curve.

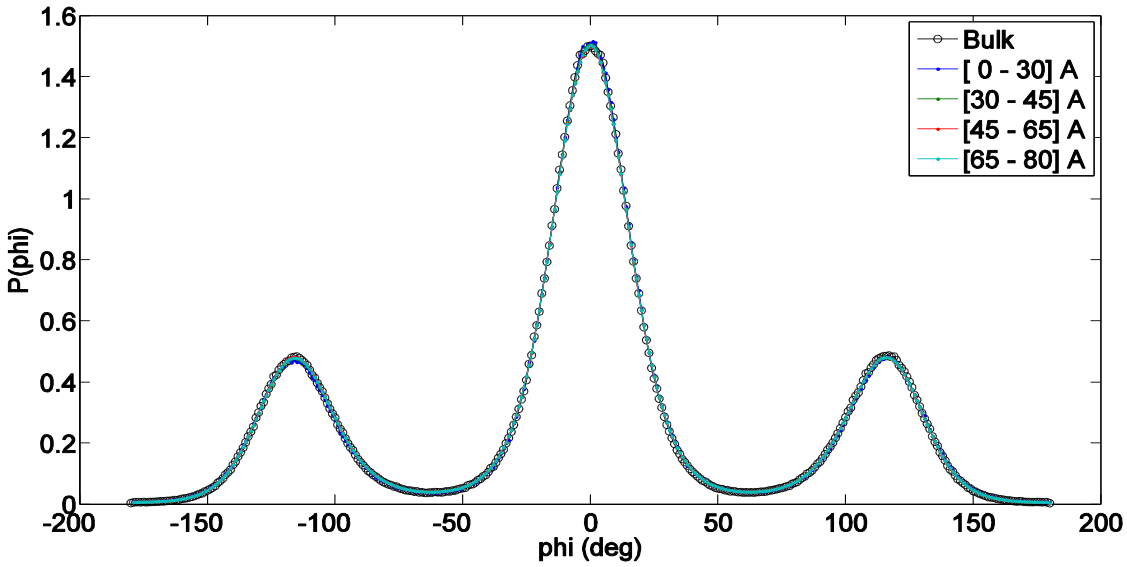

Figure 16: Torsional angles distribution as a function of R distance (distance from the center of the gold NP). All spherical shells of the (S4) system and the corresponding bulk curve.

5.4 Orientational Dynamics

We continue the analysis of the hybrid model by presenting dynamical properties of PE as a function of the distance from the Au NP. In this section we present results about the orientational dynamics, whereas I the next one the translational dynamical behavior of the model polymer chains is examined.

5.4.1 Segmental Orientational Dynamics

We start the analysis of the dynamics of polymer chains in model polymer/nanoparticle systems by studying their segmental orientational dynamics. To achieve this we use the time autocorrelation function (ACF) of the second Legendre polynomial:

$$P_2(t) = \frac{3}{2}\left\langle \cos^2 \theta(t) \right\rangle - \frac{1}{2} \tag{41}$$

We first study the orientational dynamics at the segmental level. In more detail we define the $\boldsymbol{v}^{1-3}$ vector, as previously in the analysis of the chains orientation at the monomeric level and $\theta(t)$ is the angle of this vector at time t relative to its position at $t = 0$. Results for the autocorrelation function, $P_2(t)$ are presented in Figure 17 for all hybrid PE/Au nanoparticles systems. Corresponding data for a bulk PE system are

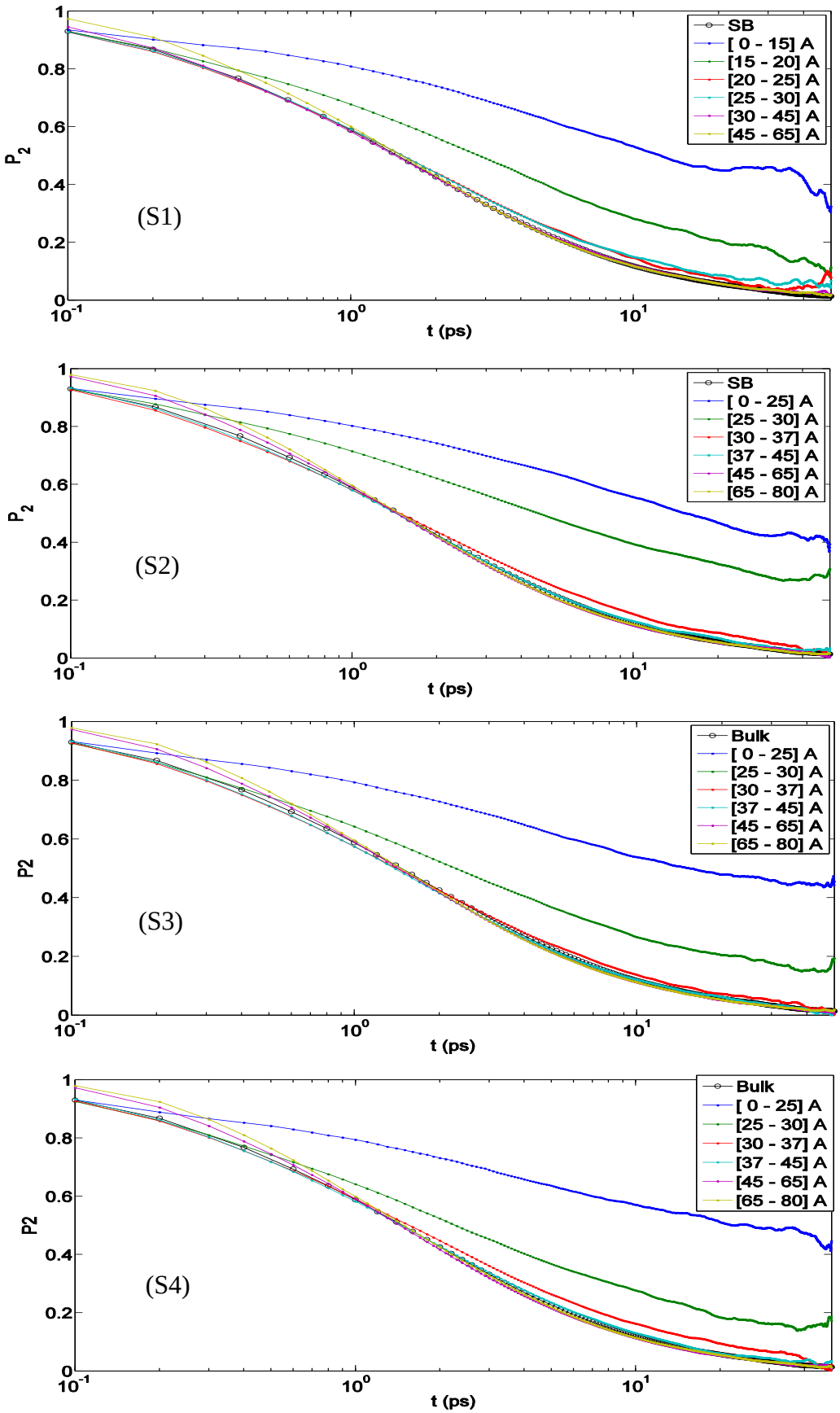

Figure 17: Time autocorrelation function (ACF) of bond order parameter $P_2(t)$ as a function of time for the characteristic vector v^{1-3} of polyethylene for all systems. $P_2(t)$ values for the S1, S2, S3 and S4 systems, for various spherical shells.

shown in these Figures as well. Note that for these calculations we monitor the position of each segment/vector only for the time period it belongs to the corresponding analysis regime. In Figure 17 $P_2(t)$ at different radial adsorption layers (*i.e.*, different distances from the Au NP's center) for the S1, S2, S3 and S4 systems are shown. PE chains in the first adsorption layers show much slower segmental dynamics compared to the bulk one. A faster decorrelation is then observed moving away from the surface up to a specific distance, while beyond this all curves coincide. This distance determines the width of the PE/Au NP interphase for the orientational segmental dynamics.

The effect of the PE/gold nanoparticle interface on the PE segmental dynamics of each system can be further quantified by computing the corresponding chain relaxation times, through proper fits of curves shown in Figure 17, with a Kohlrausch–Williams–Watts (KWW) stretch exponential function [52] of the form:

$$P_2(t) = A\exp\left[-\left(\frac{t}{\tau_{KWW}}\right)^{\beta}\right] \tag{42}$$

where, A is a pre-exponential factor which takes into account relaxation processes at very short times (e.g., bond vibrations and angle librations), τ_{KWW} is the KWW relaxation time and β the stretch exponent, which describes the broadness of the distribution of the relaxation times (*i.e.*, the deviation from the ideal Debye behavior β = 1). Then, segmental relaxation time, τ_{seg}, is calculated as the integral of the KWW curves through:

$$\tau_{seg} = \frac{\tau_{KWW}}{\beta}\Gamma\left(\frac{1}{\beta}\right) \tag{43}$$

where Γ() is the gamma function.

The results of the above analysis for both the segmental relaxation time τ_{ee} and the β exponent for PE chains of all the simulated systems are presented in Figure 19 and Figure 18. Bulk values are also shown in these figures.

It is clear the much slower orientational dynamics (larger segmental relaxation time τ_{seg}) of PE chains that are very close to the Au NP; τ_{seg} is about 10-20 times larger than the bulk one. As expected polymer chains become more mobile as their distance

from the gold nanoparticle increases, reaching a plateau, bulk-like regime, at distances of about 1.0–1.5 nm away from the Au NP. In addition, β-exponent values of PE chains are smaller than the bulk value (~0.62), as shown in Figure 18 with black line, at the majority of all distances. The latter indicates a broader distribution of the polymer segmental dynamics, compared to the bulk one.

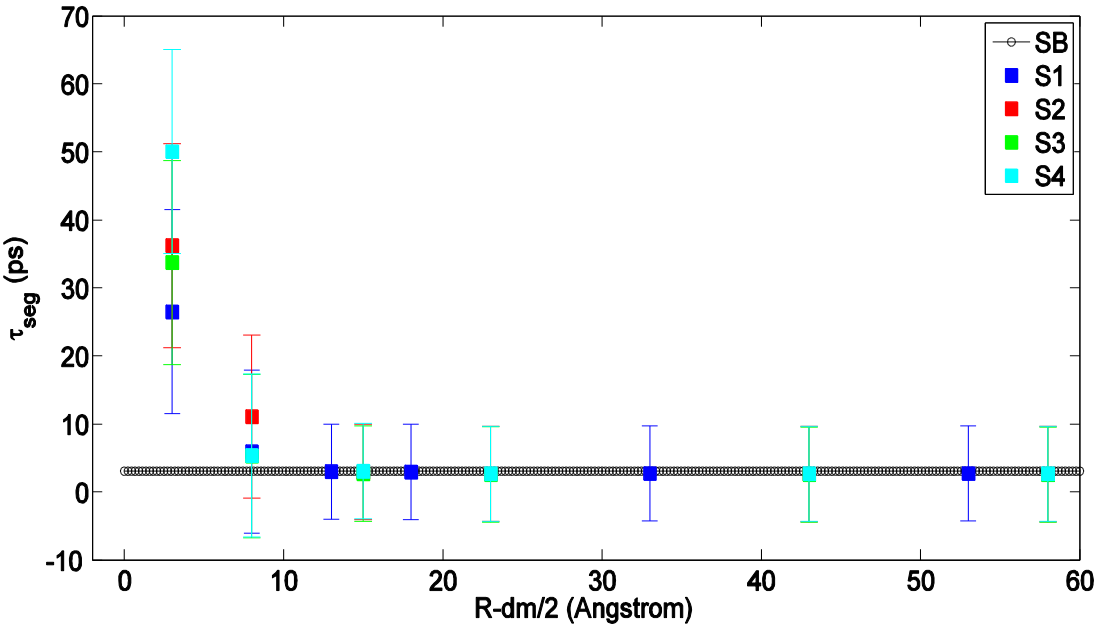

Figure 19: Segmental relaxation time, τ_{seg}, of v^{1-3} characteristic vector based on $P_2(t)$ time autocorrelation as a function of R (distance from the center of the Au NP) for all the systems. Black line represents τ_{ee} values of bulk PE under similar conditions (T = 450 K, P = 1 atm).

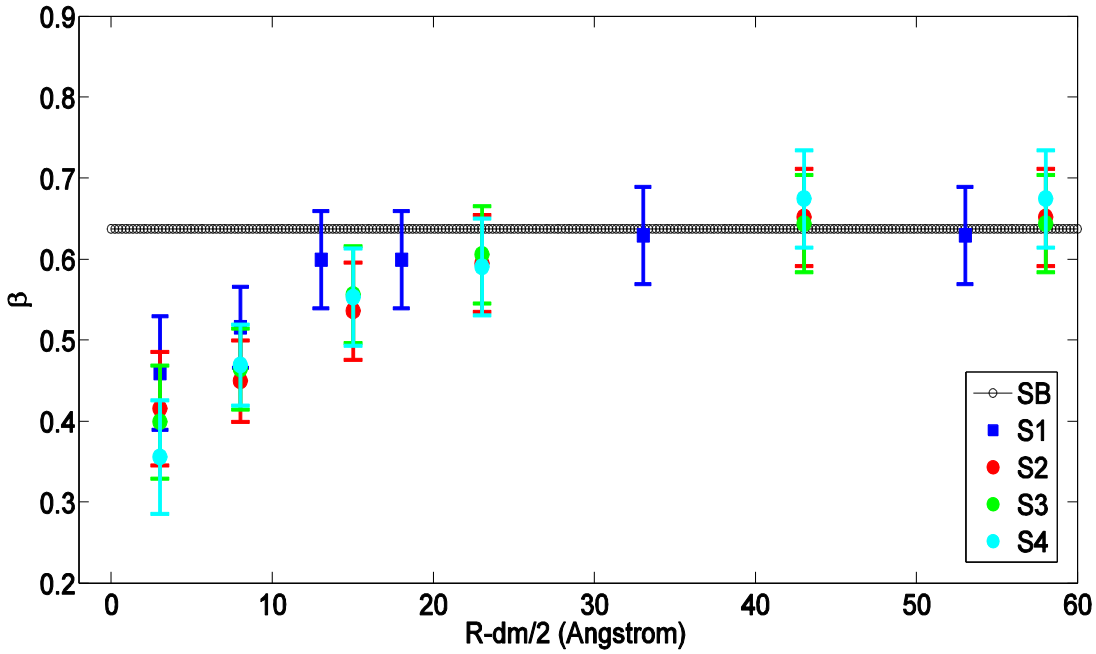

Figure 18: The stretch exponent β, as extracted from the fit with KWW functions. Black lines represent β values of bulk PE.

5.4.2 Terminal Orientational Dynamics

Next, we study the orientational dynamics at the terminal level. The $\boldsymbol{v}^{e-e}$ vector, which has been defined previously, is used. Results for the autocorrelation function, $P_2(t)$ are presented in Figure 20 and Figure 21 for all the hybrid PE/gold nanoparticles systems. Corresponding data for a bulk PE system are shown in these Figures as well. Note that for these calculations we monitor the position of each vector only for the time period it belongs to the corresponding analysis regime. In Figure 20 and Figure 21 $P_2(t)$ at different radial adsorption layers for the S1, S2, S3 and S4 systems are shown. We calculated the average value of the ACF for the entire system. The ACF for all Au NP systems are almost identical with the bulk's one due to rather small concentration of gold nanoparticles. But if we calculate the ACF as a function of the distance from the gold NP, we observe that in all systems we have slower dynamics close to the surface. PE chains in the first adsorption layers show much slower terminal dynamics compared to the bulk one. A faster decorrelation is then observed moving away from the surface up to a specific distance, while beyond this all curves coincide.

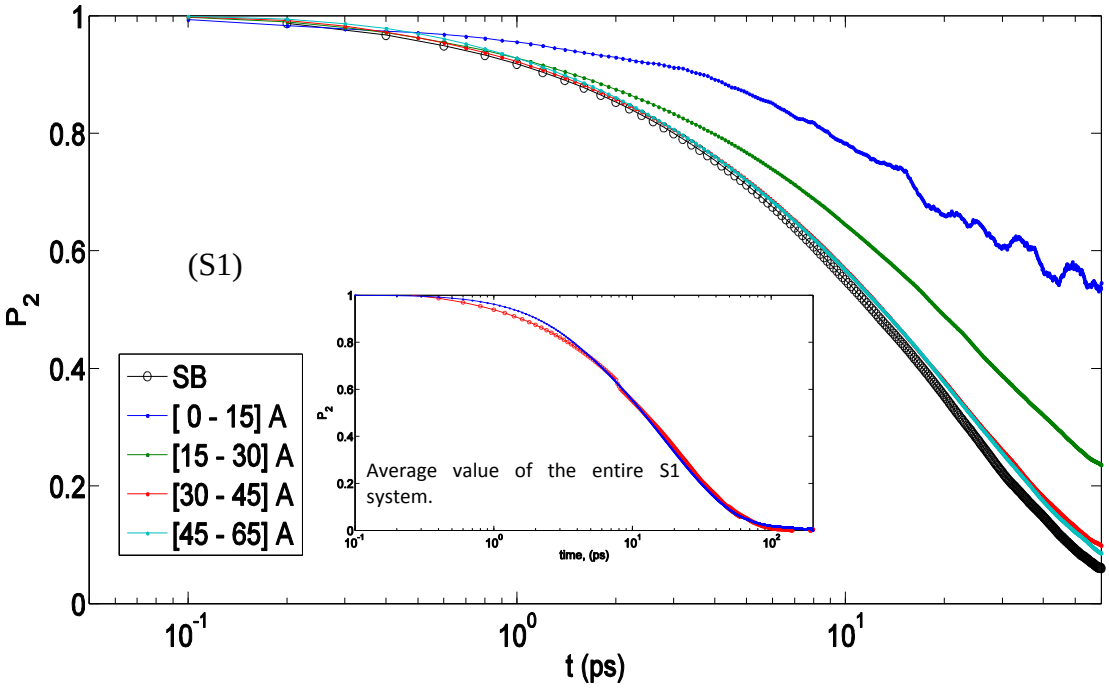

Figure 20: Time autocorrelation function (ACF) of bond order parameter P2(t) as a function of time for the characteristic vector v^{e-e} of polyethylene for S1 system. P2(t) values for the S1 system, for various spherical shells. The inset presents the average value of the entire system.

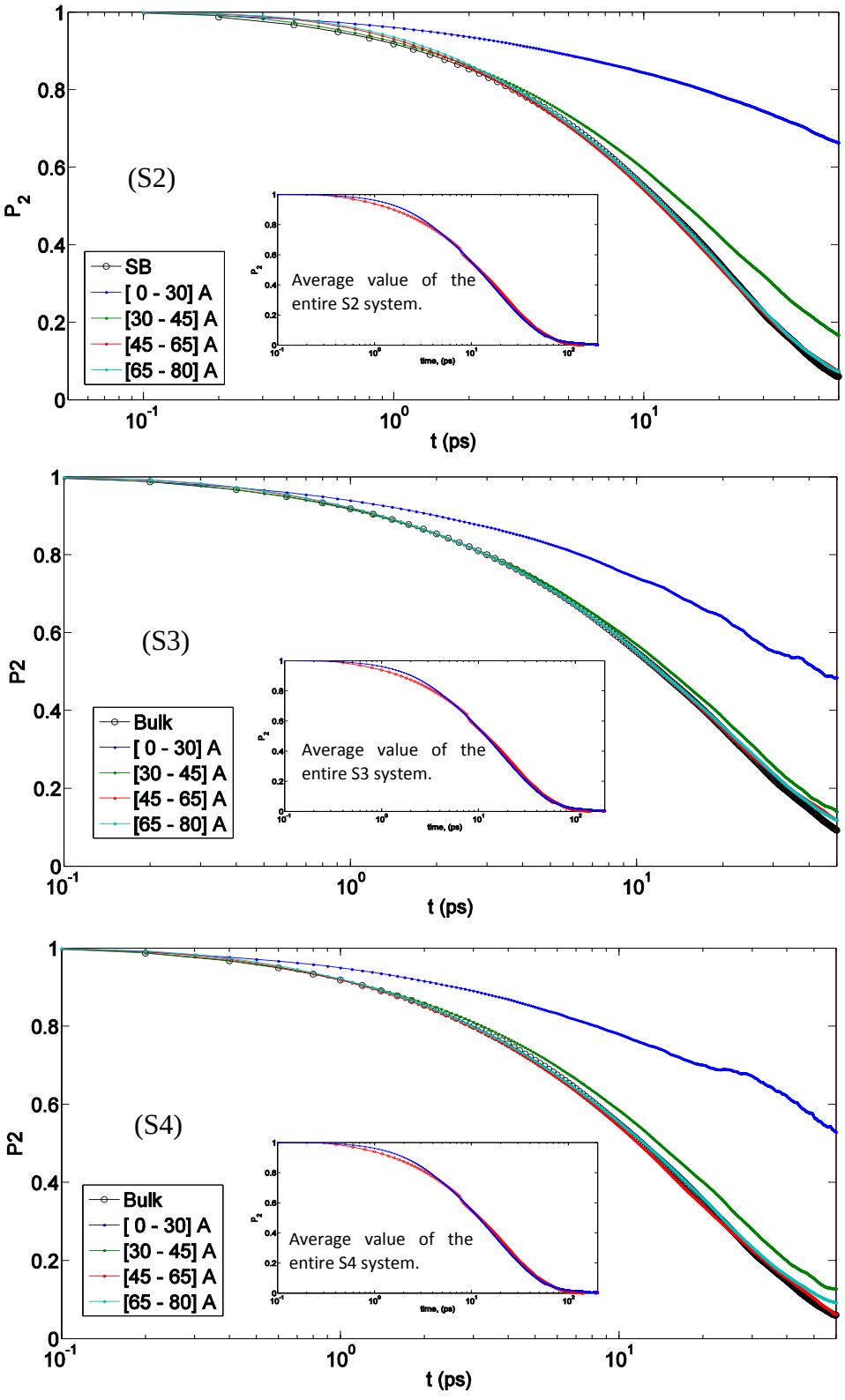

Figure 21: Time autocorrelation function (ACF) of bond order parameter P2(t) as a function of time for the characteristic vector v^{e-e} of polyethylene for S2, S3 and S4 systems. P2(t) values for the S2, S3 and S4 systems, for various spherical shells. The inset presents the average value of the entire system.

For the calculation of the chain relaxation time τ_{ee} and the β exponent, we followed the same analysis procedure as the one with the case of segmental relaxation times. Relaxation time τ_{ee} and the β exponent for PE chains, in comparison with the bulk values, of all the simulated systems are presented in Figure 22 and in Figure 23. It is clear the much slower orientational dynamics (larger terminal relaxation time τ_{ee}) of PE chains that are very close to the Au NP. Close to the Au NP we observe that PE chains have larger terminal relaxation time τ_{ee} than the bulk one. In addition, PE chains become more mobile as their distance from the gold nanoparticle increases, reaching a plateau, bulk-like regime, at distances of about 1.5–2.0 nm away from the Au NP. Furthermore, β-exponent values of PE chains are smaller than the bulk value (~0.84), as shown in Figure 23 with black line, at the majority of all distances.

The latter indicates a broader distribution of the polymer terminal dynamics, compared to the bulk one, even for distances far away from the Au NP, where the average τ_{ee} is similar to its bulk value. Therefore, when the way that polymer/gold NP interfaces affect the dynamical properties of a polymer nanoparticle system is considered, average properties do not provide the full information, but rather the whole distribution of terminal dynamics should be examined. We should also state here that if someone examines the average dynamics of all polymer chains then this is very close to the bulk one. The reason is the rather small concentration of gold nanoparticles studied here.

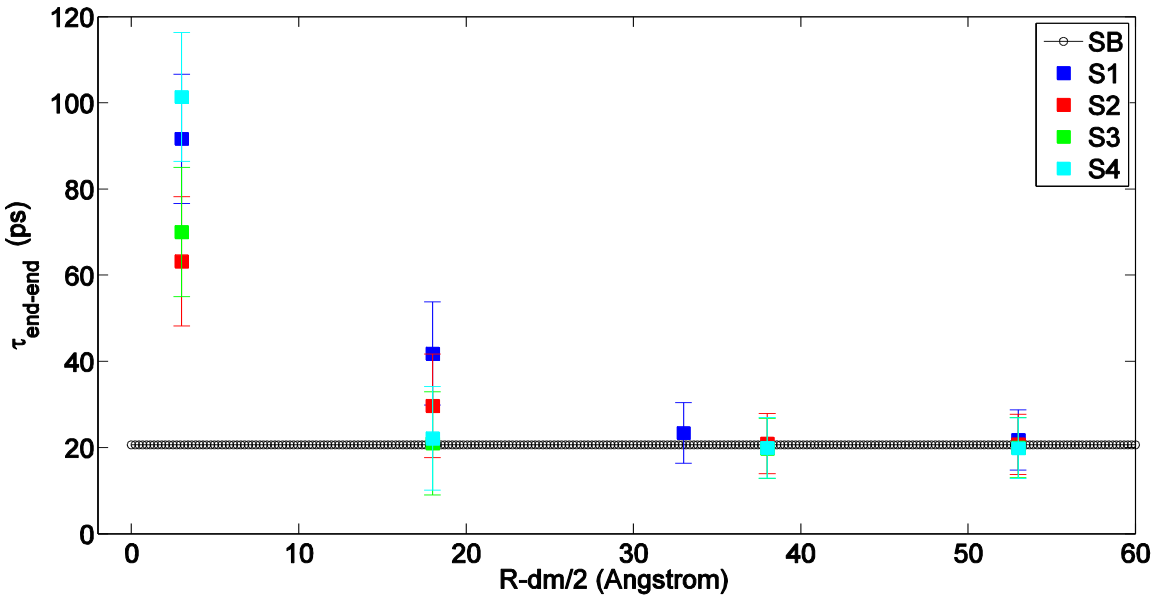

Figure 22: Terminal relaxation time, τ_{ee}, of v^{e-e} characteristic vector based on $P_2(t)$ time autocorrelation as a function of R (distance from the center of the Au NP) for all the systems. Black line represents τ_{ee} values of bulk PE under similar conditions (T = 450 K, P = 1 atm).

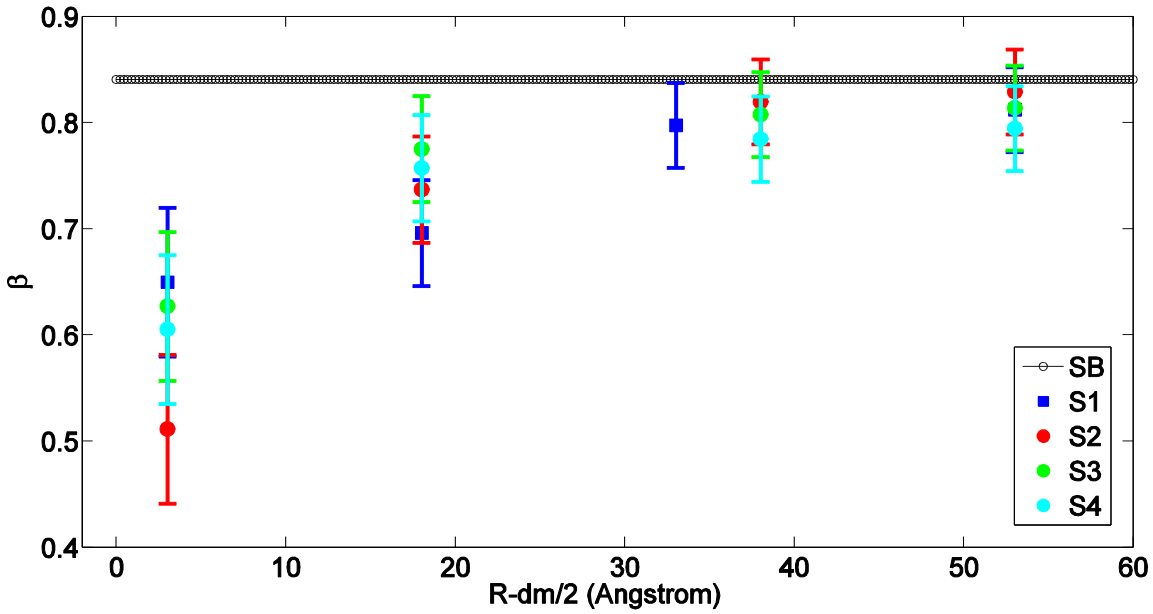

Figure 23: The stretch exponent β, as extracted from the fit with KWW functions. Black lines represent β values of bulk PE.

5.5 Translational Dynamics

5.5.1 Segmental Translational Dynamics

In the next stage, we examine the translational segmental dynamics of PE chains. To distinguish translational dynamics for different layers we have calculated the average segmental Mean-Square Displacement (MSD) defined as:

$$g^{j}(\tau) = \left\langle \left[\mathbf{r}_i(t+\tau) - \mathbf{r}_i(t) \right]^2 \right\rangle \tag{44}$$

where j is a specific radial region, i is a particular segment (CH_2 or CH_3 group here) within region j, $\mathbf{r}_i(t)$ and $\mathbf{r}_i(t + \tau)$ are the coordinate vectors of segment i at time t and $t + \tau$, respectively, whereas brackets $< >$ denotes statistical average. Note, that in the analysis used here a segment i contributes to the above average MSD for a given time interval τ and for a radial region j, if and only if it was constantly present in that region in the entire course of time τ. In Figure 24 data concerning $g^j(\tau)$ for all (radial)

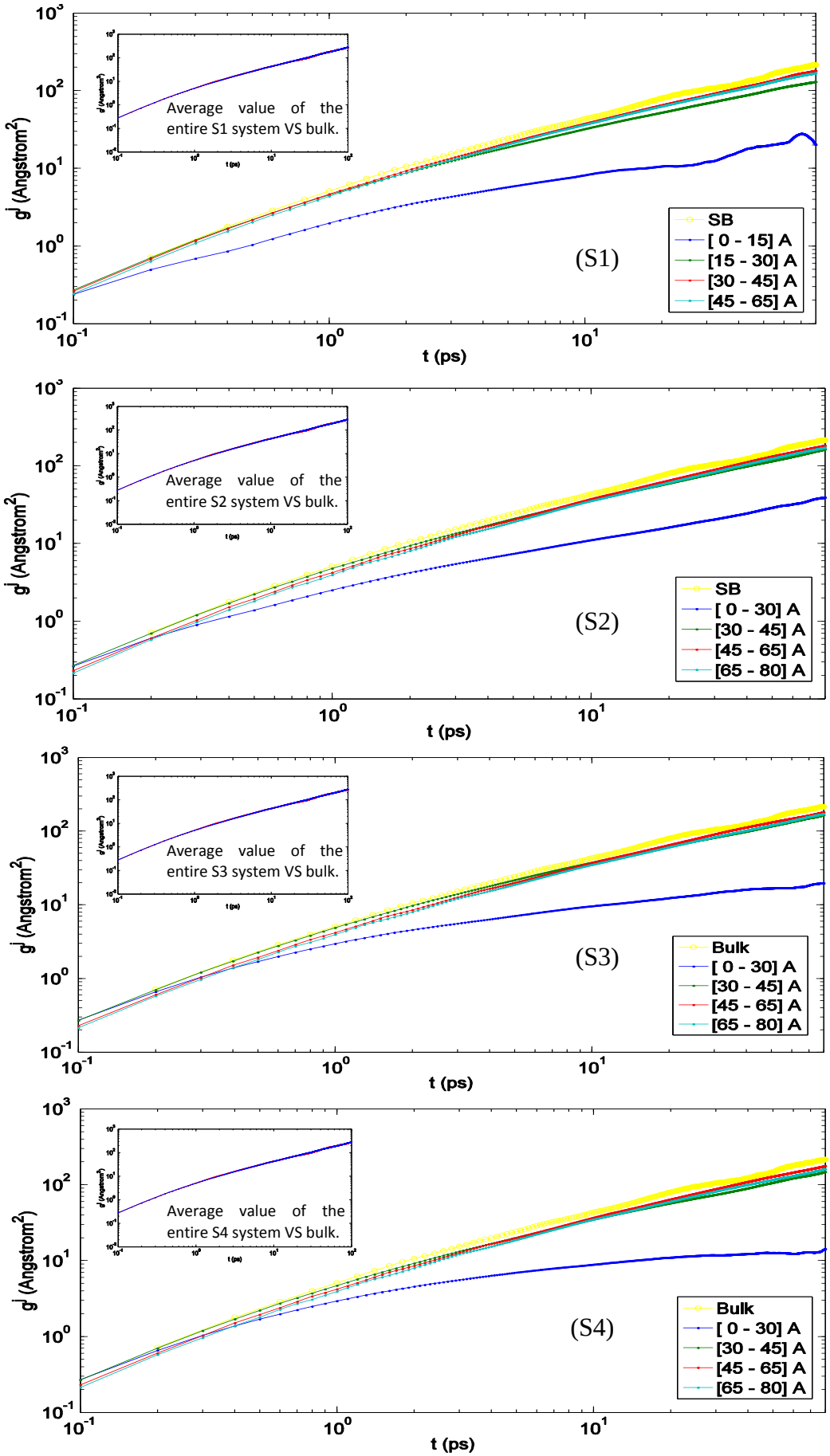

Figure 24: Segmental mean squared displacement for polyethylene chains along *R* (distance from the center of the gold NP). Values for the SB, S1, S2, S3 and S4 systems, for various spherical shells. The inset presents the average MSD value of the entire system.

adsorption layers for all the simulated systems are shown. The segmental dynamics of the polymer atoms that are closer to the Au NP atoms (mainly in the first adsorption layer) is slower compared to the one of the atoms in the other layers. On the contrast, segments belonging to the other regimes, (above second layer) exhibit rather similar dynamics, which is almost equal to the bulk one, shown in Figure 24 with yellow line. The average MSD value of the entire system is identical to the bulk's one (see insets in figures) due to small concentration of gold NPs.

5.5.2 Center of Mass Translational Dynamics

Next, we examine the translational center of mass dynamics of PE chains trough Mean-Square Displacement. The Mean-Square Displacement of the gold nanoparticle systems, as an average value of the entire system, is identical with the bulk's one (Figure 25). The reason is the rather small concentration of gold nanoparticles studied here. In Figure 26 $g^j(\tau)$ MSD data for PE chains belonging to different radial layers from the gold NP are shown for all systems (The insets in figures present the average MSD value of the entire system.). It is clear that the center of mass dynamics of the PE chains closest to the Au NP is slower, compared to the bulk one, for all hybrid model systems. The curves that belong to further spherical shells from the gold nanoparticle almost coincide with bulk's MSD.

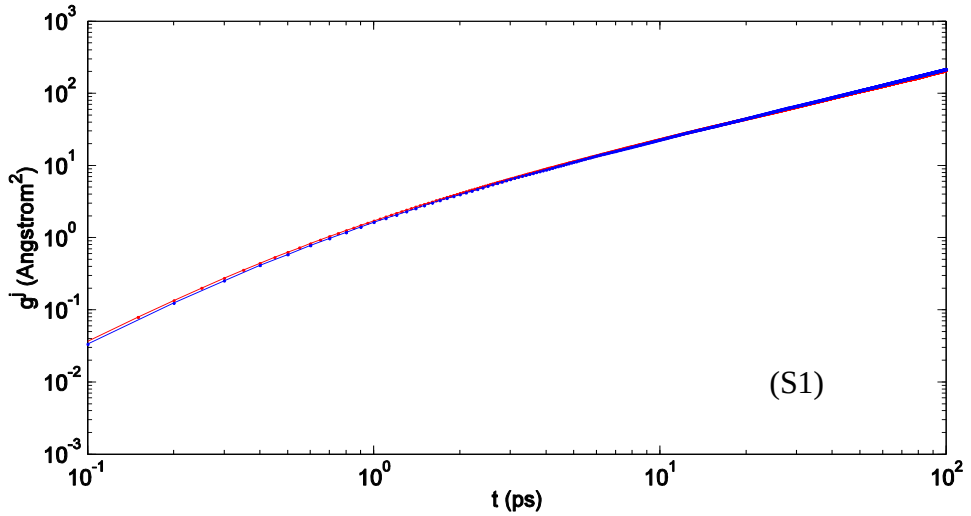

Figure 25: Center of Mass Mean-Squared Displacement average value of the entire S1 system for Polyethylene chains. With red and blue is the MSD value for the SB and S1 system respectively.

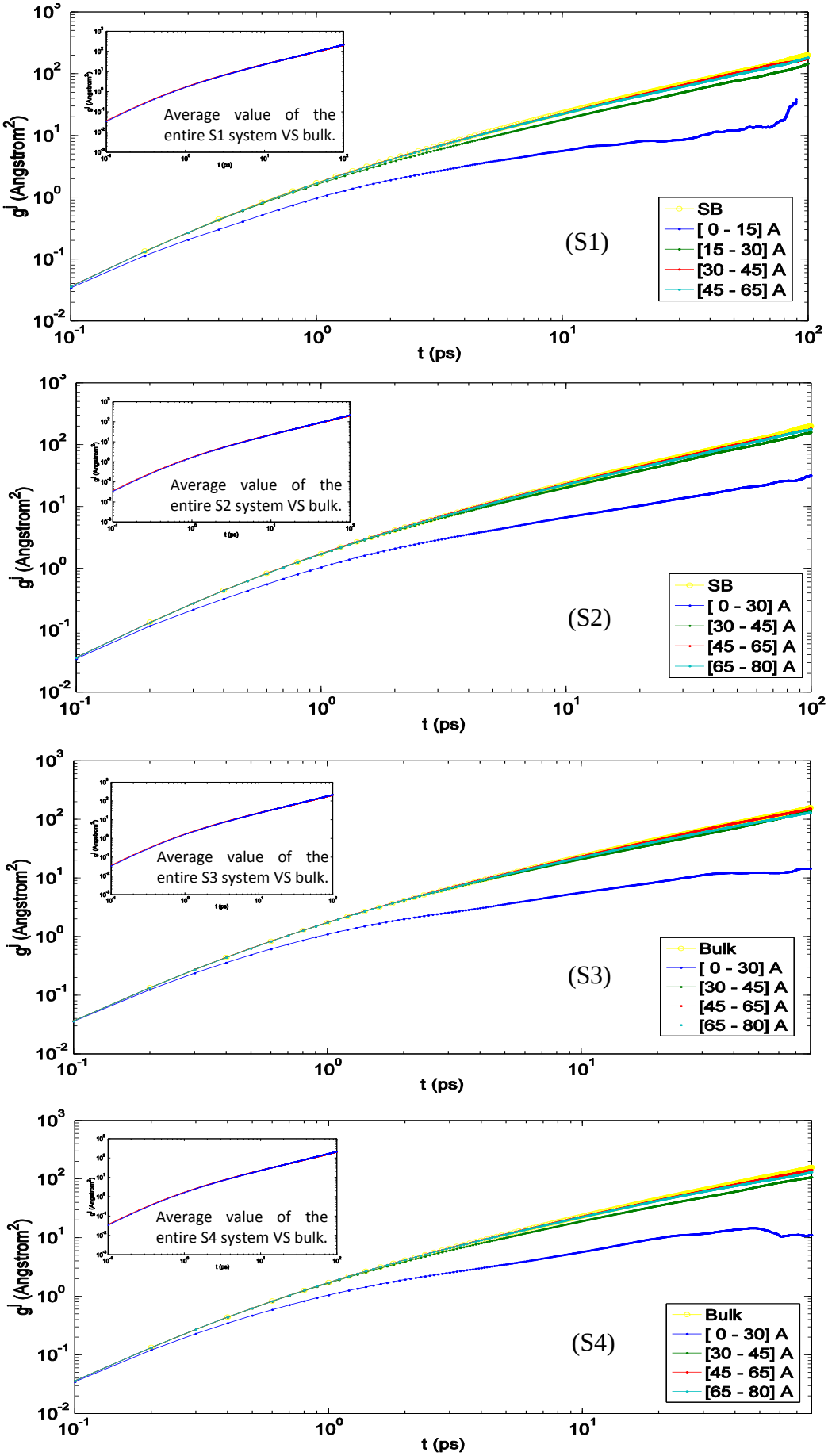

Figure 26: Center of Mass Mean-Squared Displacement for Polyethylene chains along *R* (distance from the center of the gold NP). Values for the SB, S1, S2, S3 and S4 systems, for various spherical shells. The inset presents the average MSD value of the entire system.

The mobility of the polymer in the molecular level can be described from an effective time-dependent self-diffusion coefficient, given by the following formula:

$$D(t) = \frac{\langle (r(t) - r(0))^2 \rangle}{6t} \tag{45}$$

D(t) describes the translational motion and its calculation is based on the center of mass of the polymer chain (r is the position of the chain's center of mass). For a homogeneous molecular system, exhibiting linear diffusion, D(t) reaches a constant time-independent value (self-diffusion coefficient), for times longer than about the maximum relaxation time of the molecule (polymer chain here). Figure 27 and Figure 28 presents diffusion coefficients as a function of time for all hybrid systems with the corresponding bulk curve, for various spherical shells. For all systems, the time dependent behavior of D(t) does not reach a plateau value because the polymer chains remain for short times in the spherical shells. The curves that belong to further spherical shells from the Au NP, almost coincides with bulk's D(t). Furthermore, Figure 29 display the R dependence of D(t) for various times. We observe that close to gold NP surface and for all characteristic times, dynamics is slower in comparison to the bulk one for all hybrid systems. Moreover, at short distances for the characteristic time of 1 ps dynamics is observed to be faster than that for the other two characteristic times. This can be attributed to the fact that for the time of 1 ps polymer chains move in a restricted regime which is not enough in order to be extensively affected by the existence of the surface. In contrast, away from the surface, characteristic times of 20 and 30 ps have faster dynamics compared to the 1 ps case due to longer time intervals that the chains diffuse into the corresponding spherical shells.

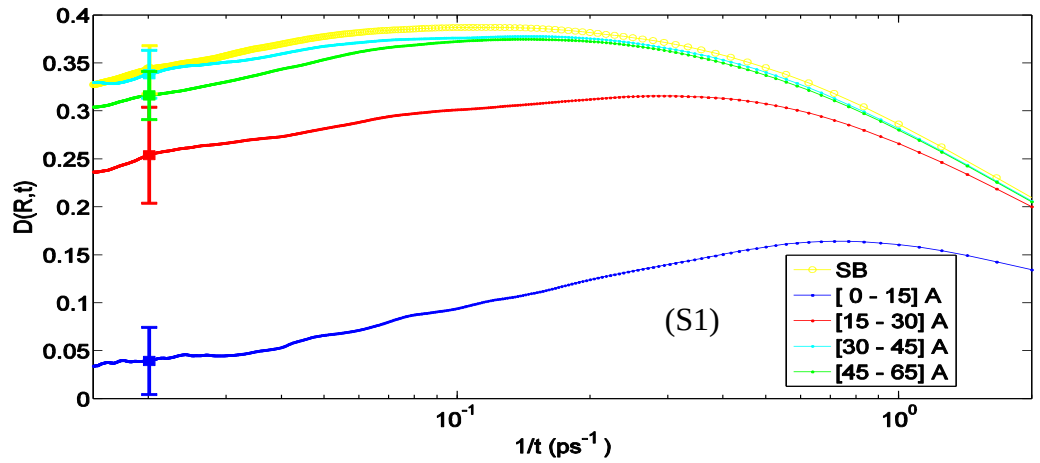

Figure 27: Time-dependent self-diffusion coefficient of the chain centers of mass for S1 and for the corresponding bulk system for various spherical shells.

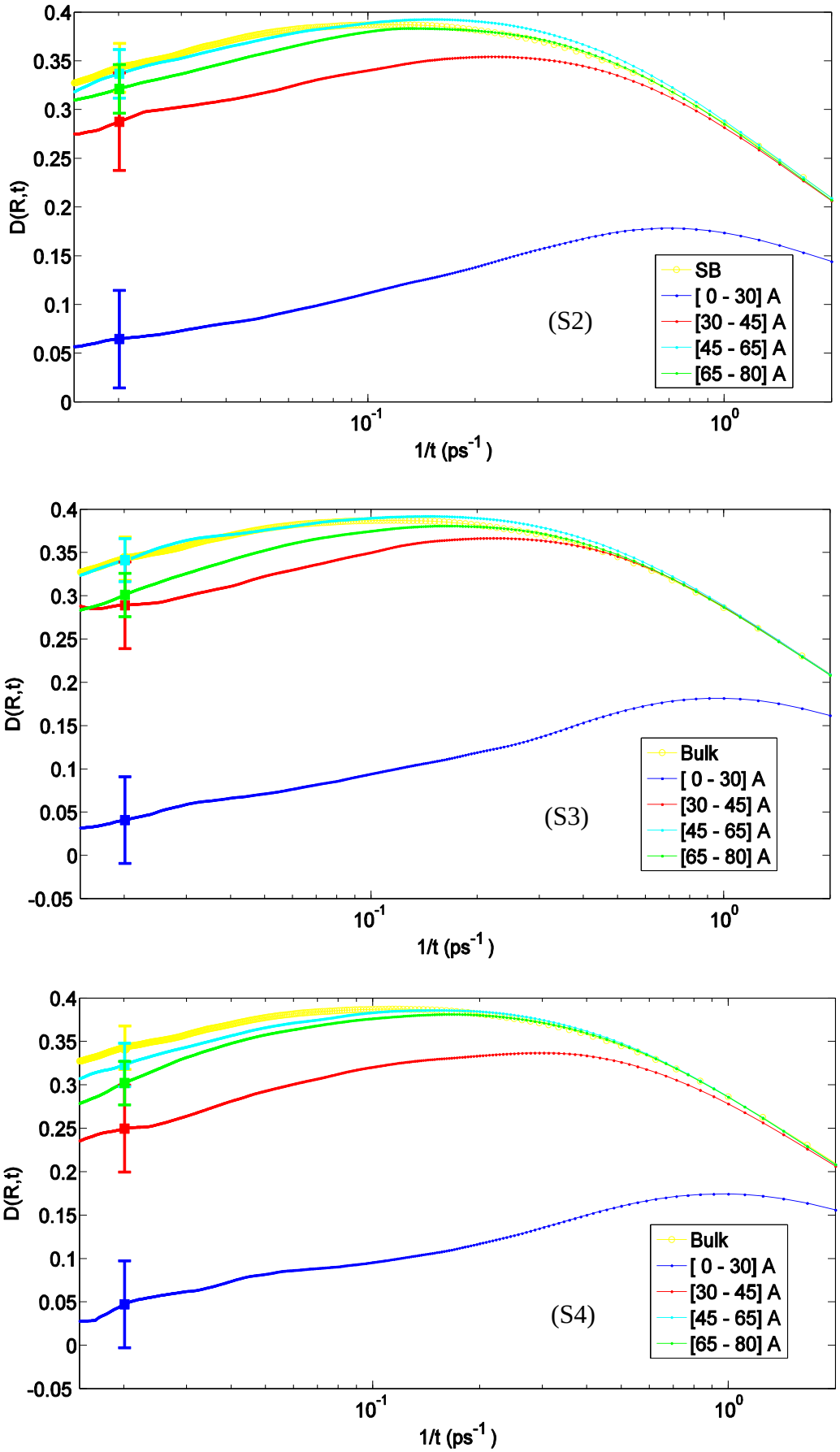

Figure 28: Time-dependent self-diffusion coefficient of the chain centers of mass for S2, S3, S4 and for the corresponding bulk system for various spherical shells.

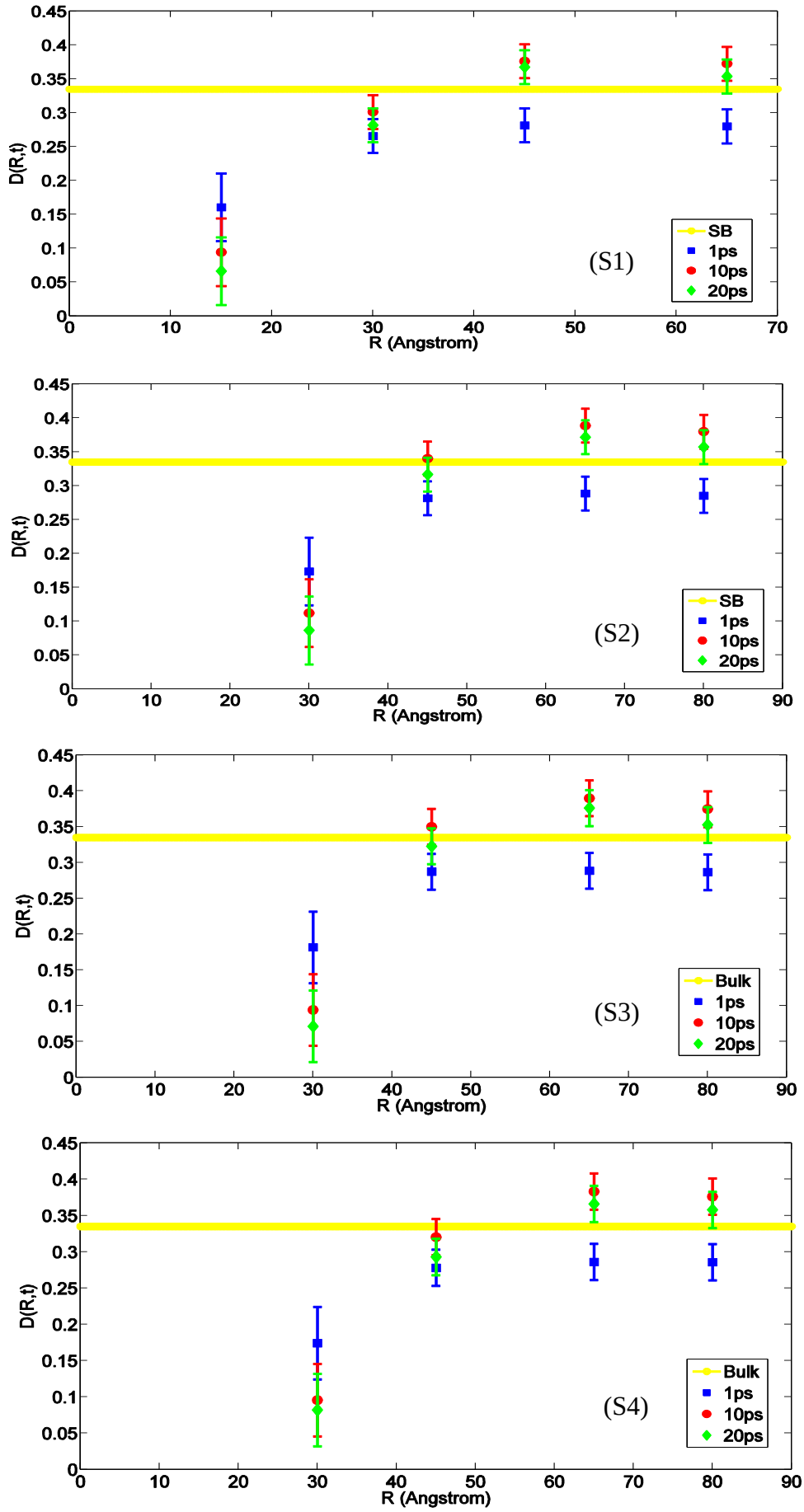

Figure 29: R (distance from the center of the gold NP) dependence of D(t) for various times for all systems.

6. CONCLUSIONS - FUTURE WORK

We studied, through detailed atomistic MD simulations, the effect of the Au NP and the Core/Shell Au NP on the structural and dynamical properties of polyethylene systems.

The behavior of polyethylene is affected by the spatial heterogeneities induced by the presence of PE/Au NP interfaces. Overall properties of the hybrid systems are almost like the bulk ones, due to the rather low concentration of gold NP. A detailed analysis was proposed based on averaging over atoms (or chains) within radial spherical shells equidistant from the center of the gold NP which allows us to examine the way that spatial heterogeneities are related to structural and dynamical features of the hybrid system as a function of distance from the polymer/gold nanoparticle interface.

From our analysis we founded that Au NP attracts polymers at distances close to it. Moreover, for the case of the Core/Shell NPs the brushes change gold NP's behavior/properties and especially the density profile. Furthermore, all systems attain bulk value in all properties away from the Au NP's surface. Results can be summarized as follows:

- Local **structural** and **conformational** features were analyzed at the level of both individual segments (atoms or bonds) and entire chains. The local monomer PE mass density near the gold surface exhibits a maximum due to the intermolecular PE/Au NP (adhesive) interaction. Chain segments show a tendency for an almost parallel to the Au NP orientation at short distances which is gradually randomized as one moves away from the interface. In addition, increase of "trans" population in the dihedral angle distribution at the PE/gold NP interface compared to the bulk one has been observed, which reflects the more ordered polymer chain structures.

- **Orientational** relaxation of PE chains in the hybrid systems at the segmental and terminal level was quantified through the time autocorrelation function of the second Legendre polynomial. Qualitatively similar behavior was found for all systems: PE chains closest to the Au NP show much slower orientational dynamics (segmental relaxation time τ_{seg} is about 10 times larger) compared to

the bulk one. Faster $P_2(t)$ decorrelation is observed moving away from the interface up to a specific distance, while beyond this, all curves coincide. In addition, broader distribution of the polymer orientational dynamics, compared to the bulk one was found (smaller β-exponent values).

- **Translational** segmental and center of masses dynamics of PE chains was examined through the calculation of the average mean-square displacement. PE chains closest to the Au NP are slower, compared to the bulk one, for all model hybrid systems, due to the polymer/gold nanoparticle interfaces.

In Table 4 we summarize the effect of interface on various properties.

Effect of Interface:	
Density	**1.0 – 2.5 nm**
Structural	**1.0 - 1.5 nm**
Local (segmental) dynamics	**0.5 – 1.5 nm**
Global dynamics	**2.0 – 4.0 nm**

Table 4: The effect of interface on various properties.

Current work concerns the calculation of the potential of mean force (PMF) between two gold NPs. In addition, we examine the properties, of the studied here, hybrid systems as a function of polyethylene molecular length and temperature. In a future work we want to develop a Coarse Grain (CG) model for those hybrid systems.

REFERENCES

1. Kotelyanskii, M. and D.N. Theodorou, *Simulation Methods for Polymers.* Marcel Dekker Inc., New York, USA, 2004.

2. Frenkel, D. and B. Smith, *Understanding Molecular Simulations: From Algorithms to Applications.* Academic Press: New York, 1996.

3. Allen, M.P. and D.J. Tildesley, *Computer simulation of liquids.* Oxford Science, Oxford, 1987.

4. Doi, M. and S.F. Edwards, *The Theory of Polymer Dynamics.* Claredon: Oxford, 1986.

5. Anastasiadis, S., et al., Macromolecules, 2011. **44**.

6. Oh, H. and P.F. Green, Nature Materials, 2009. **8**: p. 139 - 143.

7. Moniruzzaman, M. and K.I. Winey, *Polymer Nanocomposites Containing Carbon Nanotubes.* Macromolecules, 2006. **39**(16): p. 5194-5205.

8. Breen, T.L., et al., Science, 1999. **284**(948).

9. Priestley, R.D., et al., Science, 2005. **309**.

10. Anastasiadis, S., et al., Phys. Rev. Lett., 2000. **84**.

11. Ma, J.-z., et al., *Research advances in polymer emulsion based on "core–shell" structure particle design.* Advances in Colloid and Interface Science, 2013. **197–198**(0): p. 118-131.

12. Dhoke, S.K. and A.S. Khanna, *Study on electrochemical behavior of Nano-ZnO modified alkyd-based waterborne coatings.* Journal of Applied Polymer Science, 2009. **113**(4): p. 2232-2237.

13. Laachachi, A., et al., *Effect of ZnO and organo-modified montmorillonite on thermal degradation of poly(methyl methacrylate) nanocomposites.* Polymer Degradation and Stability, 2009. **94**(4): p. 670-678.

14. Dashtizadeh, A., et al., *Acrylic coatings exhibiting improved hardness, solvent resistance and glossiness by using silica nano-composites.* Applied Surface Science, 2011. **257**(6): p. 2118-2125.

15. Che, X.-C., Y.-Z. Jin, and Y.-S. Lee, *Preparation of nano-TiO2/polyurethane emulsions via in situ RAFT polymerization.* Progress in Organic Coatings, 2010. **69**(4): p. 534-538.

16. Zhu, A., et al., *Synthesis of core–shell PMMA–SiO2 nanoparticles with suspension–dispersion–polymerization in an aqueous system and its effect on mechanical properties of PVC composites.* Polymer Testing, 2008. **27**(5): p. 540-547.

17. Wen, X.-f., et al., *Study of the physicochemical properties of silica powder and the stability of organic–inorganic hybrid emulsion in the presence of ethanol.* Colloids and Surfaces A: Physicochemical and Engineering Aspects, 2008. **327**(1–3): p. 103-110.

18. Binder, K., *Monte Carlo and Molecular Dynamics Simulations in Polymer Science.* Oxford University Press: New York, 1995.

19. Mansfield, K.F. and D.N. Theodorou, Macromolecules, 1991. **24**.

20. Rissanou, A.N. and V. Harmandaris, *Structural and Dynamical Properties of Polystyrene Thin Films Supported by Multiple Graphene Layers.* Macromolecules, 2015. **48**(8): p. 2761-2772.

21. Rissanou, A., A. Power, and V. Harmandaris, *Structural and Dynamical Properties of Polyethylene/Graphene Nanocomposites through Molecular Dynamics Simulations.* Polymers, 2015. **7**(3): p. 390-417.

22. Rissanou, A. and V. Harmandaris, *Dynamics of Polymer/Graphene Interfacial Systems.* Soft Matter, 2014. **10**: p. 2876-2888.

23. Harmandaris, V.A., et al., *Atomistic molecular dynamics simulation of diffusion in binary liquid n-alkane mixtures.* The Journal of Chemical Physics, 2002. **116**(17): p. 7656.

24. Xia, T.K., et al., Phys. Rev. Lett., 1992. **69**.

25. Matsuda, T., et al., Macromolecules, 1995. **28**.

26. Mischler, P.C., et al., Polymer, 2002. **43**.

27. Ayoagi, T., J. Takimoto, and M. Doi, J. Chem. Phys., 2001. **115**.

28. Johnson, K. and V. Harmandaris, *Properties of short polystyrene chains confined between two gold surfaces through a combined density functional theory and classical molecular dynamics approach.* Soft Matter, 2012. **8**: p. 6320-6332

29. Kim, Y., R.C. Johnson, and J.T. Hupp, *Gold Nanoparticle-Based Sensing of "Spectroscopically Silent" Heavy Metal Ions.* Nano Letters, 2001. **1**(4): p. 165-167.

30. Boisselier, E. and D. Astruc, *Gold nanoparticles in nanomedicine: preparations, imaging, diagnostics, therapies and toxicity.* Chemical Society Reviews, 2009. **38**(6): p. 1759-1782.

31. Lal, S., S. Link, and N.J. Halas, *Nano-optics from sensing to waveguiding.* Nat Photon, 2007. **1**(11): p. 641-648.

32. Lu, Y., et al., *Synthesis and Self-Assembly of Au@SiO2 Core−Shell Colloids.* Nano Letters, 2002. **2**(7): p. 785-788.

33. Barmparis, G.D. and I.N. Remediakis, *Dependence on CO adsorption of the shapes of multifaceted gold nanoparticles: A density functional theory.* Phys. Rev. B, 2012. **86**(085457).

34. Ciccoti, G. and W.G. Hoover, *Molecular Dynamics Simulations of Statistical Mechanics Systems.* Proceedings of the 97th Int. Enrico Fermi School of Physics, North Holland, Amsterdam, 1986.

35. Harmandaris, V.A., *Atomistic Molecular Dynamics Simulations of Polymer Melt Viscoelasticity.* Ph.D. Thesis, University of Patras, 2002.

36. Harmandaris, V.A., et al., *Molecular Dynamics Simulations of Polymers, Chapter in Book Simulation Methods for Polymers.* Marcel Dekker, New York, 2004.

37. Goldstein, H., *Classical Mechanics.* Addison-Wesley, MA, 1980.

38. Plimpton, S., *Fast Parallel Algorithms for Short-Range Molecular Dynamics.* J Comp Phys, 1995. **117**: p. 1-19.

39. Nosé, S., Mol. Phys., 1984. **52**(255).

40. Hoover, W.G., Phys. Rev. A, 1985. **31**(1695).

41. Andersen, H.C., J. Chem. Phys., 1980. **72**(2384).

42. Parinello, M. and A. Rahman, Phys. Rev. Lett., 1980. **45**(1196).

43. Power, A.J., *Molecular Dynamics Simulations with Long Range Interactions.* Thesis, University of Crete, 2011.

44. Remediakis, I.N., N. Lopez, and J.K. Nørskov, *CO oxidation on gold nanoparticles: Theoretical studies.* Applied Catalysis A: General, 2005. **291**(1–2): p. 13-20.

45. Remediakis, I.N., N. Lopez, and J.K. Nørskov, *CO Oxidation on Rutile-Supported Au Nanoparticles.* Angewandte Chemie International Edition, 2005. **44**(12): p. 1824-1826.

46. Kopidakis, G., et al., *Atomic and electronic structure of crystalline–amorphous carbon interfaces.* Diamond and Related Materials, 2007. **16**(10): p. 1875-1881.

47. Hadjisavvas, G., I.N. Remediakis, and P.C. Kelires, *Shape and faceting of Si nanocrystals embedded in a-SiO2: A Monte Carlo study.* Physical Review B, 2006. **74**(16): p. 165419.

48. Herring, C., Phys. Rev. A, 1951. **82**(87).

49. Hautman, J. and M.L. Klein, J. Chem. Phys., 1989. **91**.

50. Alexiadis, O., et al., *Atomistic Simulation of Alkanethiol Self-Assembled Monolayers on Different Metal Surfaces via a Quantum, First-Principles Parametrization of the Sulfur-Metal Interaction.* J. Phys. Chem. C, 2007. **111**.

51. Turzi, S.S., *On the Cartesian definition of orientational order parameters.* J. Math. Phys., 2011. **52**.

52. Williams, G. and D.C. Watts, *Non-symmetrical dielectric relaxation behaviour arising from a simple empirical decay function.* Trans. Faraday Soc., 1970. **66**(80-85).